Chemical Reviews

Volume 94, Number 8 December 1994

# Shrink-Wrapping an Ion Cloud for High-Performance Fourier Transform Ion Cyclotron Resonance Mass Spectrometry

Shenheng Guan, Hyun Sik Kim, and Alan G. Marshall*

*National High Magnetic Field Laboratory and Department of Chemistry, Florida State University, Tallahassee, Florida 32306*

Markus C. Wahl

*Department of Chemistry, The Ohio State University, Columbus, Ohio 43210*

Troy D. Wood

*Department of Chemistry, Cornell University, Ithaca, New York 14853*

Xinzhen Xiang

*The R. W. Johnson Pharmaceutical Research Institute, Spring House, Pennsylvania 19477*

*Received May 25, 1994 (Revised Manuscript Received September 7, 1994)*

## Contents



* Correspondong author: Prof. Alan G. Marshall, National High Magnetic Field Laboratory, Florida State University, 1800 East Paul Dirac Dr., Tallahassee, FL 32306-4005.

## I. Introduction

Fourier transform ion cyclotron resonance mass spectrometry (FT-ICR/MS or FTMS) is a powerful analytical tool capable of ultrahigh mass-resolving power, precise mass measurement, multistage MS/MS, high mass range, ion remeasurement, simultaneous detection of all ions, and long ion storage time. The principles, applications, and current developments of analytical FT-ICR/MS have been thoroughly reviewed.[1-27] Although the stated advantages of FT-ICR/MS are true and have been achieved individually or in certain combinations in various experiments, full realization of those advantages for analytical and bioanalytical applications has often been limited by the wide radial distribution of ions in an ICR ion trap. This article offers the first review of the ion axialization method, a newly developed technique which solves the radial distribution problem and greatly generalizes the above-stated advantages of FT-ICR/MS.

All FT-ICR experiments are conducted in an ICR ion trap which is enclosed in a high-vacuum chamber. A high-performance FT-ICR/MS spectrometer is typi-

0009-2665/94/0794-2161$14.00/0 

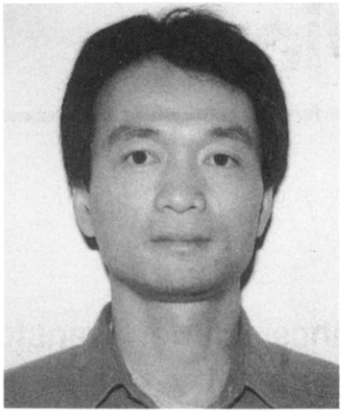

Shenheng Guan received a B.S. in chemistry in 1982 from Fudan University, Shanghai, China, and did two years of graduate research in theoretical chemistry in Dalian Institute of Chemical Physics, Chinese Acedemy of Sciences. He received his Ph.D. degree in 1989 at University of the Pacific in Physical/Analytical Chemistry based on design and construction of an FT-ICR mass spectrometer. Following postdoctoral research on instrumentation and applications of Fourier transform mass spectrometry and biological mass spectrometry at University of California Irvine, University of California, San Francisco, and The Ohio State University, Dr. Guan assumed the position of Associate Director of the ICR program at the National High Magnetic Field Laboratory in Tallahassee, FL. His current research includes physics of trapped ions and analytical applications of high performance mass spectrometry.

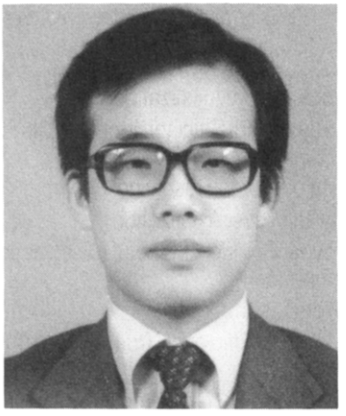

Hyun Sik Kim received his B.S. and M.S. in 1983 from Seoul National University, Seoul, Korea. From 1986 to 1989, he was a member of the Faculty Board in the Korea Air Force Academy and in 1989 was a research associate in the Department of Chemistry at the Pohang Institute of Science and Technology, Pohang. He is currently a Ph.D. candidate in Physical Chemistry with Professor Marshall at The Ohio State University, focusing on the physics of trapped ions and analytical applications of FT mass spectrometry and surface chemistry. In the ICR program at the National High Magnetic Field Laboratory at Florida State University, he is helping to develop techniques for optical spectroscopy of mass-selected ions.

cally equipped with a horizontal-bore superconducting solenoidal magnet with a field induction of 3−7 T. The vacuum chamber is placed inside the magnet bore so that the ICR trap is located in the most spatially homogeneous central magnetic field region.

The frequency, $\nu_c$ (in hertz, Hz), of the well-known circular cyclotron motion of an ion in a plane perpendicular to the magnetic field is (in the absence of the electrical potential) inversely proportional to mass-to-charge ratio, $m/q$, of the ion, $\nu_c = (qB)/(2\pi m)$ (SI units), in which $m$ and $q$ are the mass and charge of the ion, and $B$ is the magnetic field induction. The ion mass-to-charge ratio (usually expressed as m/z, in which m is mass in unified atomic mass units (u) and z is the number of elementary charges per ion) may thus be obtained

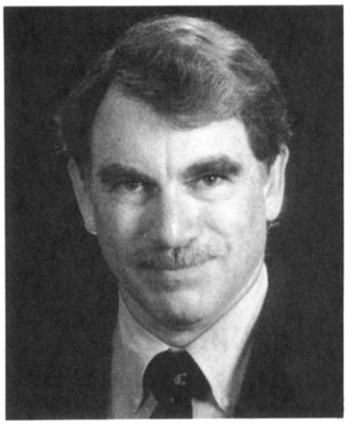

Alan G. Marshall, born in Ohio in 1944, received his B.A. degree in Chemistry from Northwestern University in 1965 and Ph.D. in Physical Chemistry from Stanford University in 1970. He joined the Chemistry faculty at the University of British Columbia (Vancouver, Canada) in 1969, moved to The Ohio State University in 1980 as Professor of Chemistry and Biochemistry and Director of the Campus Chemical Instrument Center, and to the National High Magnetic Field Laboratory at Florida State University in 1993 as Professor of Chemistry and Director of the ICR Program. Over the past 25 years, his research interests have shifted from NMR (line-shape analysis and macromolecular structure determination) to mass spectrometry. He is best known for his co-invention (with M. B. Comisarow) and continuing development of Fourier transform ion cyclotron resonance mass spectrometry, for which he won the ACS Akron Section Award and the OSU Distinguished Scholar Award in 1988, was elected to the rank of Fellow in both the American Physical Society and the American Association for the Advancement of Science in 1989, and received the ACS Division of Analytical Chemistry Award in Chemical Instrumentation in 1990, the Eastern Analytical Symposium Award in Analytical Chemistry in 1991, and (jointly with Comisarow) the 1995 American Chemical Society Field-Franklin Award in Mass Spectrometry. His comprehensive book, *Fourier Transforms in NMR, Optical, and Mass Spectrometry*, co-authored with F. R. Verdun, appeared in 1990.

Markus C. Wahl was born in 1967 in Göttingen, Germany. He studied Biochemistry at the University of Hannover, Germany, and the University of Rochester, NY, before enrolling in the graduate program in Biochemistry with Professor Marshall at The Ohio State University in 1991, working on axialization of laser desorbed/ionized biomolecules for FT-ICR mass analysis. After receiving his M.S. in Biochemistry there in 1993, he switched to macromolecular cyrstallography, and is currently working toward his Ph.D. in Biochemistry with Professor M. Sundaralingam at The Ohio State University.

from measurement of the unperturbed cyclotron frequency, $\nu_c$, of the ion.

Trapping of ions in the presence of a strong magnetic field and a three-dimensional quadrupolar electrostatic potential is the foundation of virtually all FT-ICR experiments. Figure 1 shows the approximately quadrupolar trapping potential generated by the commonly used cubic ICR trap.[28] In the (axial) direction of the magnetic field, the potential

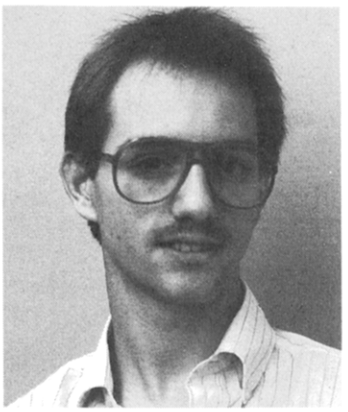

Troy D. Wood, born in 1967 in Indiana, received his B.S. with Honors in Chemistry from Indiana University in 1989. He completed his Ph.D. in Analytical Chemistry with Professor Marshall at The Ohio State University in 1993, concentrating mainly on improved techniques for laser desorption/ionization FT-ICR mass spectrometry for analysis of fullerenes and other species. He is presently a postdoctoral research associate in Fred W. McLafferty's laboratory at Cornell University, where he is investigating the structures of biological macromolecules with electrospray FT-ICR mass spectrometry.

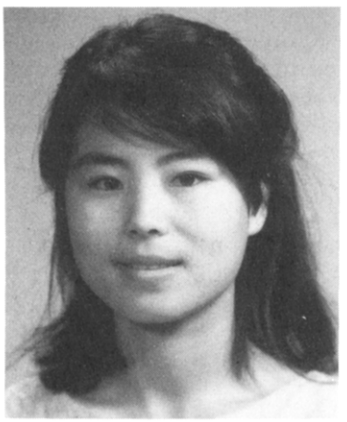

Xinzhen (Jane) Xiang received her B.S. in Chemistry from Zhejiang University in China in 1984, and Ph.D. from The Ohio State University in 1993. Her Ph.D. research with Professor Marshall ranged from FT-ICR mass analysis of phosphite additives to dehydrogenation of cyclic alkanes by $Os^+$, and she also developed a general program for numerical simulation of ion trajectories for virtually any ICR experiment. Currently, she is a Research Scientist at the R. W. Johnson Pharmaceutical Research Institute, where her primary research is directed at methods development of LC/MS/MS of drugs and biomolecules.

is parabolic with a *minimum* at the center of the trap. However, on the transverse midplane ($z = 0$), the potential is an inverted parabola with a *maximum* at the center of the trap. In the absence of a time-varying electric excitation field, ion motions may be considered to be a combination of three independent motions, namely cyclotron, magnetron, and axial motions (see Figure 2).[29] The cyclotron frequency of an ion in a quadrupolar electrostatic trapping potential is shifted downward relative to $\nu_c$, and the center of the cyclotron motion drifts along an isopotential contour due to the $\mathbf{E} \times \mathbf{B}$ force, in which $\mathbf{E}$ is the electrostatic trapping field and $\mathbf{B}$ is the magnetic field induction. The drift circular motion, or magnetron motion, is nearly independent of m/z ratio of the ion and (except at very high m/z) is much lower in frequency than $\nu_c$. Ion axial motion is a simple linear harmonic oscillation whose frequency is inversely proportional to $(m/z)^{1/2}$.

If energy dissipation mechanisms are not provided, these three motions are bounded and ions remain trapped. However, ions can lose energy in many ways in real FT-ICR experiments. Collisional damping is the most common way for ions to lose energy. The initial amplitudes of ion cyclotron and axial motions (Figure 3 top left and right) decrease with time because a smaller cyclotron radius corresponds to lower kinetic energy and a smaller $z$ amplitude corresponds to lower kinetic and potential energy. Although the magnetron orbit is stable in the absence of collisions or other mechanisms for ion energy loss, collisional damping causes the magnetron radius to expand since a large magnetron radius corresponds to lower (trapping) potential energy (Figure 3, top middle). Ions gradually migrate radially toward the electrodes parallel to the magnetic field and are eventually lost from the trap.

For various FT-ICR/MS experiments, however, it is important to be able to trap ions at high neutral gas pressure for an extended period. For example, tandem mass spectrometry[30] is conducted most effectively by use of collision-induced dissociation which requires a high-collision gas pressure for ion activation. A unique feature of FT-ICR/MS is its capability to remeasure high-mass ions, an experiment which requires many collisions to relax the ions back to the center of the trap for reexcitation.[31] Ion internal energy needs to be reduced prior to accurate measurement of ion−molecule reaction rate constants: a large number of collisions may be needed to remove vibrational energy of an ion.[19] High-mass ions of great biological interest may be generated by matrix-assisted laser desorption ionization (MALDI)[32−34] in which ions have high kinetic energy,[35] or electrospray ionization[36−38] in which ions exhibit lower (but wider distribution in) kinetic energy. High and/or a distribution in ion kinetic energy is undesirable for high-resolution ICR detection. Collisional damping is the most efficient method for reducing ion kinetic energy. It is apparent that a method that could prevent or even reverse the magnetron expansion process would be highly desirable for extending the utility of FT-ICR/MS.

As an aside, it is interesting to note that the current success of the quadrupole ion trap (QIT) mass spectrometer is due mainly to the introduction of ion cooling at high He buffer gas pressure.[39] Unlike an ICR ion trap with its electrostatic trapping potential, the high-amplitude rf driving voltage applied to the ring electrode of the QIT forms a so-called pseudopotential which has an energy minimum at the center of the trap. Loss in energy by collisions causes ions to relax to positions near the center of the trap.

The ion axialization method summarized in this article originated in the field of atomic physics, in which confinement of charged particles in a small volume in space is of great interest for precise measurements of fundamental properties of the particles. One of the most successful methods is use of a Penning trap to isolate one or a few electrons or atomic ions for a prolonged period (hours to months).[29] For low-mass charged particles in a Penning trap, such as electrons and protons, direct measurement of cyclotron motion is difficult because the cyclotron frequency is high and because the ion must be excited to such a large radius that the relativistic mass shift becomes significant (e.g., $^3He^+$ at a cyclotron radius

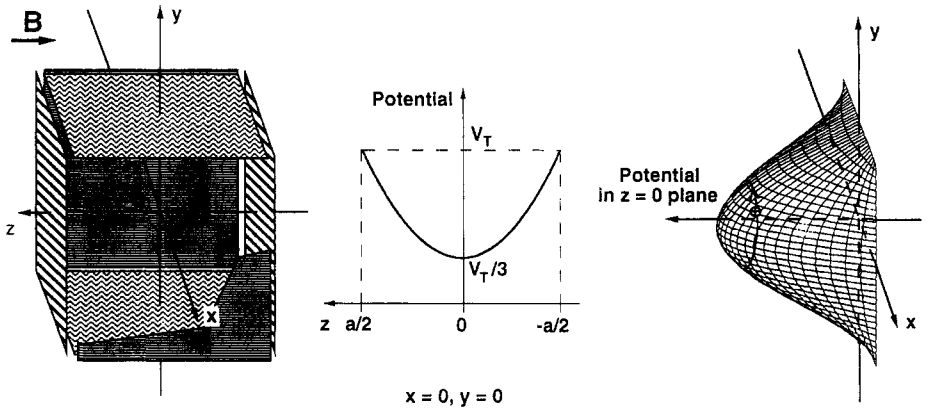


**Figure 1.** Axial (left) and radial (right) electrostatic trapping potential in a cubic ICR ion trap. Along the magnetic field ($z$) direction, the trapping potential is parabolic, with its minimum at the center of the trap. In the trap $z = 0$ midplane perpendicular to the magnetic field, the "bell-shape" potential surface (approximately parabolic near the trap center) has a maximum at the center of the trap.

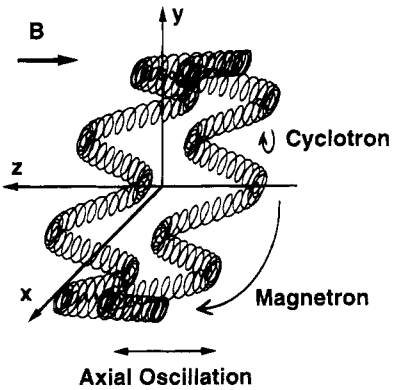


**Figure 2.** Natural motions of ions in a pure quadrupolar electrostatic trapping potential. In the absence of a time-varying electric excitation field, there are three independent natural periodic motions: cyclotron (small circles), magnetron (along an electric equipotential line such as that shown in the right-hand diagram of Figure 1), and trapping (sinusoidal oscillation in the $z$ direction).

of ~1 cm at 7 T travels at ~1% of the speed of light!). Therefore, most Penning trap measurements are based on detection of ion axial oscillation at much lower frequency and much lower ion speed. Cyclotron and magnetron motions are detected indirectly by virtue of their coupling to the (directly detectable) axial motion. Although the electrodes of a Penning trap may be machined to near-perfect hyperboloids of revolution, the electrostatic potential nevertheless deviates significantly from a pure quadrupolar potential when ions move away from the center of the trap, due to truncation of the trap (to finite dimensions) and because of holes in the electrodes to admit or expel ions. It is therefore necessary to confine the ions near the center of the trap. The cyclotron radius of an electron may be reduced by radiation damping. Resistive damping of the current induced in the end cap electrodes by the electron axial motion dissipates the axial oscillation energy and lowers the axial amplitude. However, these energy loss mechanisms also cause the magnetron radius to expand. Wineland and Dehmelt first proposed a method to couple magnetron motion to the resistively damped axial motion to reduce the magnetron radius.[40,41] The coupling was achieved by application of an excitation potential of $xz$ symmetry at the combined frequency, $\omega_z + \omega_-$, in which $\omega_z$ is the axial oscillation frequency and $\omega_-$ is the magentron frequency (see below). Van Dyck, Schwinberg, and Delmelt developed a "sideband cooling" method based on the same principle.[42] The cooling method has become standard for single-ion Penning trap or "geonium" spectroscopy.[29]

One could also think of coupling the magnetron motion to the damped cyclotron motion to reduce the magnetron radius. Brown and Gabrielse proposed that cooling of magnetron motion by coupling to cyclotron motion in a Penning trap could be achieved by splitting the ring electrode and applying a quadrupolar $xy$ excitation potential at frequency, $\omega_+ + \omega_-$, in which $\omega_+$ is the cyclotron frequency.[29] The coupling of magnetron and cyclotron motions was later studied in more detail by Bollen *et al.*[43]

All of the above methods are based on resistive damping (or laser cooling) which is ineffective for cooling heavy ions. The additional problem associated with resistive cooling is the requirement that ion motion be coherent so that significant induced current passes through a resistor. For cooling of heavy ions on the other hand, collisional damping is by far the most efficient method. Magnetron cooling by quadrupolar excitation in the presence of collisional damping was first demonstrated experimentally by Savard *et al.*[44] for ions of a single m/z ratio.

We carried out the first ion axialization with broadband ICR detection by use of a dual-trap FT-ICR mass spectrometer.[45] Ions generated in the source compartment of the dual trap were subjected to aximuthal quadrupolar excitation at the unperturbed cyclotron frequency, $\omega_c = \omega_+ + \omega_-$, of ions of the m/z of interest in the presence of a high pressure of buffer gas. In this way, the magnetron radius of the ions could be reduced to less than the radius of the conductance limit separating the source trap from the analyzer compartment, so that axialized ions could be transferred to the analyzer for detection at much lower pressure. With the ion axialization method, prolonged trapping at high buffer gas pressure, enhanced mass-resolving power, and improved mass selectivity under high space–charge conditions for laser-desorbed ions were demonstrated.[46] Speir *et al.* later showed that ion remeasurement efficiency in a single-compartment ICR trap could be improved by pulsing collision gas during the ion axialization interval.[47] For optimal ion axialization (see below), a relatively high buffer gas pressure stable for tens of seconds is required. However, ions should be

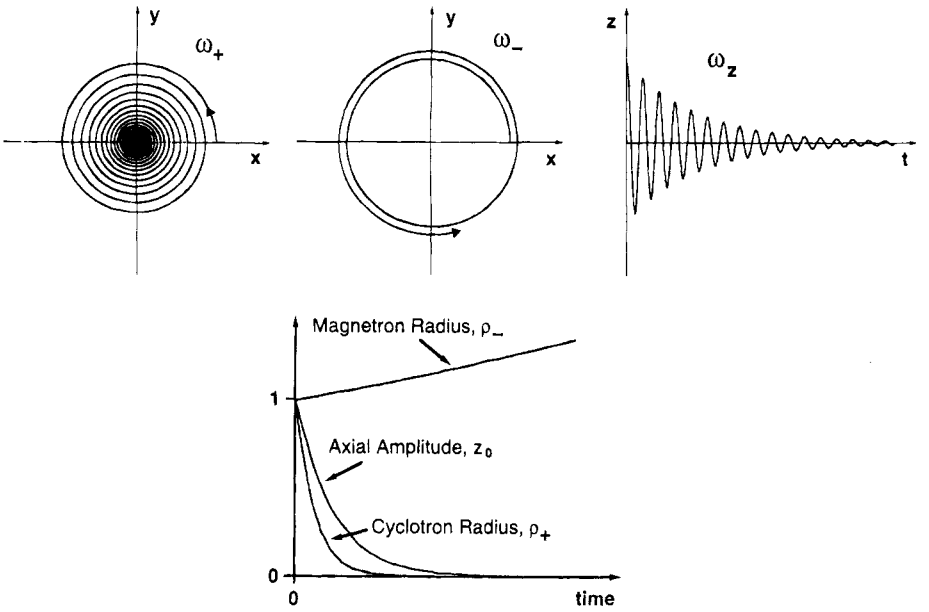


**Figure 3.** Effect of collisional damping on the three natural ion motions in an ICR ion trap. The top left shows exponential damping of cyclotron radius; top middle; exponential growth of magnetron radius; and top right, exponential damping of $z$ oscillation amplitude. The bottom shows relative time rates of change of the three motional amplitudes—note that cyclotron radius is damped about twice as fast as axial oscillation and that both are damped at rates much faster than the rate of increase of magnetron radius.

detected at the lowest pressure possible to attain high mass-resolving power. Although the dual-trap configuration allows separation of ion axialization and detection, the high pressure in the source trap causes a nonnegligible increase in pressure in the analyzer trap where ions are detected. That problem may be resolved by use of multiply pulsed buffer gas,[48] making it possible to axialize ions at nearly constant pressure and detect them at the lowest possible pressure. Mass-resolving power for laser-desorbed ions may be further improved by axialization enhanced by a "digital heterodyne frequency drift correction method".[49]

Another important aspect in development of the ion axialization method is extension of single-frequency resonant axialization of ions of just one m/z ratio to broad-band axialization over wide m/z range(s). A theoretical study[50] has shown that interconversion of magnetron and cyclotron motion is closely related to excitation of a quantum mechanical two-energy level system (e.g., spin $^1/_2$ NMR). Indeed, the equations of motion for the conversion process may be expressed in the form of the well-known Bloch equations. Therefore, excitation techniques developed for broad-band population inversion in NMR (e.g., adiabatic rapid passage, "shaped" pulses) may be adapted directly for conversion between magnetron and cyclotron motions. In practice, however, broad-band axialization can more easily be realized by use of repeated low-amplitude SWIFT azimuthal quadrupolar excitation, by analogy to NMR excitation at low "tip" angle.[51] Each of the identical SWIFT excitation pulses converts a fraction of magnetron amplitude to cyclotron amplitude which is in turn collisionally damped before the next pulse. The axialization range is defined solely by the magnitude spectrum of the SWIFT waveform, so that ions of arbitrary m/z range(s) may be axialized simultaneously.

Optimal instrumental technique development typically requires deep understanding of the underlying theoretical principles, as well as analytical and (when necessary) numerical analysis of system behavior. In this review, we offer the first comprehensive analytical treatment of the theory of resonant azimuthal quadrupolar excitation in the presence of collisional damping. Starting from the quadrupolar electrostatic ("trapping") and quadrupolar time-varying ("excitation") electric potentials in an ICR ion trap, we solve analytically the equations of ion motions in the presence of azimuthal quadrupolar excitation and collisional damping and then show how the ion trajectory depends on collisional damping rate and excitation amplitude. The present theoretical treatment of resonant azimuthal quadrupole excitation is formally very similar to that previously presented for the less common $xz$ excitation,[52] and its inclusion here is justified by the much more general interest and importance of azimuthal ($xy$) quadrupolar excitation. We also show how to relate the phases of the cyclotron and magnetron motions as a result of the magnetron/cyclotron interconversion process. Finally, in the Applications section, we offer representative examples illustrating the various advantages of the new axialization technique.

## II. Quadrupolar Excitation Potential and Equations of Ion Motion

The classical motion of an ion of mass, $m$, and charge, $q$, moving at velocity, $\mathbf{v}$ ($=\dot{x}\mathbf{i} + \dot{y}\mathbf{j} + \dot{z}\mathbf{k}$), in a magnetic field, $\mathbf{B}$, and electric field, $\mathbf{E}$, in the presence of collisional damping force proportional to ion velocity is described by the modified Lorentz equation (SI units)[53,54]

$$m\dot{\mathbf{v}} = q(\mathbf{E} + \mathbf{v} \times \mathbf{B}) - m\gamma\mathbf{v} \qquad (1)$$

In most FT-ICR experiments, $\mathbf{B}$ is constant and spatially homogeneous, and its direction may be used to define the $z$ axis ($\mathbf{B} = -B\mathbf{k}$). $\gamma$ is the collision damping rate constant ($s^{-1}$). The electric field, $\mathbf{E}$, may be determined from the potential, $\Phi$, inside the trap

$$\mathbf{E} = -\nabla\Phi \tag{2}$$

In the absence of Coulomb interactions, the electric potential is determined by the Laplace equation

$$\nabla^2\,\Phi(x,y,z) = \left(\frac{\partial^2}{\partial x^2} + \frac{\partial^2}{\partial y^2} + \frac{\partial^2}{\partial z^2}\right)\Phi(x,y,z) = 0 \tag{3}$$

subject to boundary conditions defined by the ICR ion trap geometry (see below).

## A. Electrostatic Trapping Potential

Different ICR ion trap designs variously optimize excitation and/or detection electric field uniformity to suppress[55-58] or amplify[59-61] signals at harmonic frequencies, and/or linearize[62,63] or zero[64] the axial electrostatic trapping field. However, as we shall show, a simple cubic trap[28] offers the best overall compromise for generating an approximately three-dimensional quadrupolar electrostatic potential for ion trapping, an approximately spatially uniform aximuthal dipolar time-varying electric field for excitation and detection of ion cyclotron motion, and an approximately azimuthal quadrupolar time-varying electric potential for conversion of magnetron motion to cyclotron motion. Positive ions may be confined in a cubic ICR ion trap by applying a voltage, $V_T$ (positive relative to the remaining electrodes) to the pair of opposed trapping electrodes perpendicular to the magnetic field direction. The boundary conditions for such a conventional trapping potential in a cubic trap of edge length, $a$ (see Figure 1) are

$$\Phi_T = \begin{cases} V_T & z = \pm a/2 \\ 0 & x = \pm a/2 \text{ or } y = \pm a/2 \end{cases} \tag{4}$$

Equation 3 may be solved subject to the above boundary conditions by the variable separation method[65]

$$\Phi_T(x,y,z) = \frac{16V_T}{\pi^2}\sum_{n=0}^{\infty}\sum_{m=0}^{\infty}\left[\left[(-1)^{m+n} \times \cos\left[\frac{(2n+1)\pi x}{a}\right]\cos\left[\frac{\pi(2m+1)y}{a}\right] \times \cosh\left[\frac{\pi z\sqrt{(2n+1)^2+(2m+1)^2}}{a}\right]\right]\Big/\left[(2n+1) \times (2m+1)\cosh\left[\frac{\pi\sqrt{(2n+1)^2+(2m+1)^2}}{2}\right]\right]\right] \tag{5}$$

Taylor expansion of eq 5 through third order in $x$, $y$, and $z$ about the trap center ($x = y = z = 0$) yields the much simpler approximate expression

$$\Phi_T \approx V_T\left[\gamma' - \frac{\alpha}{2a^2}(x^2 + y^2 - 2z^2)\right] \tag{6}$$

in which $V_T$ is the "trapping" voltage applied to the trapping plates, $a$ is the trap edge length, and $\gamma'$ and $\alpha$ are trap geometry factors: $\gamma' = 1/3$ and the second-order Taylor expansion coefficient, $\alpha$, is 2.77373 for a cubic trap. Figure 1 shows the trapping potential along the $z$ axis and in a cubic ICR ion trap. For the cubic trap, Figure 1 shows that along the $z$ axis ($x = y = 0$), the potential is parabolic with a minimum value of $V_T/3$ at the trap center ($x = y = z = 0$). Figure 1 also shows that in the $xy$ midplane ($z = 0$) of the trap, the potential is maximal at the trap center and approaches zero at the "side" electrode boundary.

## B. Quadrupolar Excitation Potential in a Cubic ICR Ion Trap

As previously pointed out for azimuthal quadrupolar excitation,[50] we need to solve a Laplace problem subject to the boundary conditions

$$\Phi_{xy} = \begin{cases} V_{xy}(t) & x = \pm a/2 \\ -V_{xy}(t) & y = \pm a/2 \end{cases} \tag{7}$$

in which $V_{xy}(t)$ is the excitation voltage applied to each "side" electrode. The potential for this boundary problem may be expressed as the superposition of two potentials

$$\Phi_{xy}(x,y,z) = \Phi_1(x,y,z) + \Phi_2(x,y,z) \tag{8}$$

with boundary conditions

$$\Phi_1(x,y,z) = \begin{cases} 0 & y = \pm a/2 \text{ or } z = \pm a/2 \\ V_{xy}(t) & x = \pm a/2 \end{cases} \tag{9a}$$

and

$$\Phi_2(x,y,z) = \begin{cases} 0 & x = \pm a/2 \text{ or } z = \pm a/2 \\ -V_{xy}(t) & y = \pm a/2 \end{cases} \tag{9b}$$

$\Phi_1$ and $\Phi_2$ are antisymmetric with respect to reflection through the $x = y$ plane. Thus, to obtain the potential for the original geometry, we need only solve the Laplace equation for $\Phi_1(x,y,z)$ (eq 3). Fortunately, the above boundary problem is equivalent to that for the electrostatic potential in a cubic trap (eq 4) with interchange of the $z$ axis for the $x$ or $y$ axis.

$$\Phi_1(x,y,z) = V_{xy}(t)\left[\gamma' - \frac{\alpha}{2a^2}(z^2 + y^2 - 2x^2)\right] \tag{10a}$$

and

$$\Phi_2(x,y,z) = -V_{xy}(t)\left[\gamma' - \frac{\alpha}{2a^2}(z^2 + x^2 - 2y^2)\right] \tag{10b}$$

Addition of eqs 10a and 10b gives

$$\Phi_{xy}(x,y,z) = \Phi_1(x,y,z) + \Phi_2(x,y,z) = \frac{3\alpha V_{xy}(t)}{2a^2}(x^2 - y^2) \tag{11}$$

Figure 4 shows equipotential surfaces for three different potential configurations of an ICR ion trap of square cross section. The electrostatic potential for a cubic trap is the familiar three-dimensional hyperbolic equipotential surfaces common to ICR and quadrupole ion traps.[66] For a tetragonal ion trap extended infinitely along the axial ($z$) direction, the dipolar potential used for excitation of ion cyclotron

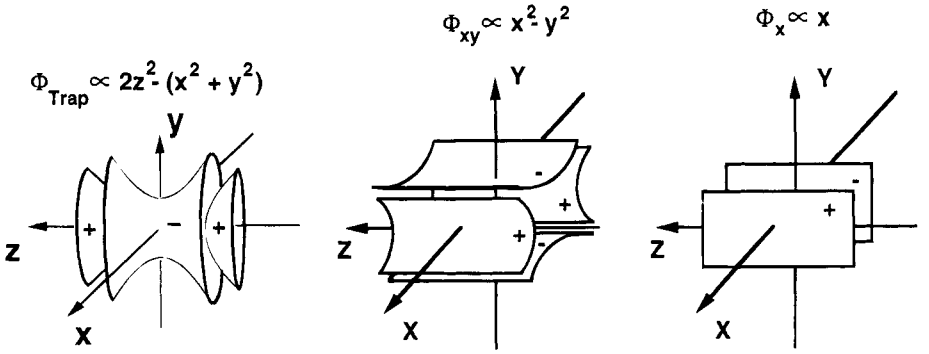


**Figure 4.** Symmetry of each of three different electrical potentials in an ICR ion trap. The left shows electrostatic trapping potential is approximately three-dimensional quadrupolar, resonant at $\omega_+$ (and $\omega_-$ and $\omega_z$); middle, time-varying electric excitation potential for magnetron/cyclotron interconversion is approximately azimuthal two-dimensional quadrupolar, resonant at $\omega_c$; right, Azimuthal dipolar excitation potential is one-dimensional spatially linear.

motion is approximately one-dimensional and the azimuthal quadrupolar excitation potential of eq 11 is two-dimensional. All three pictures represent approximate representations which become exact at the center of the trap.

## C. Equations of Ion Motion under Azimuthal Quadrupolar Excitation

During azimuthal quadrupolar excitation, the electric field is the superposition of the trapping and the excitation fields. From eqs 6 and 11,

$$\begin{aligned}\mathbf{E} &= -\nabla[\Phi_T + \Phi_{xy}] \\ &= -\nabla\left[V_T\left[\gamma' - \frac{\alpha}{2a^2}(x^2 + y^2 - 2z^2)\right] + \frac{3\alpha V_{xy}(t)}{2a^2}(x^2 - y^2)\right] \\ &= \frac{m}{2q}\omega_z^2\,[x\mathbf{i} + y\mathbf{j}] - \frac{m}{q}\omega_z^2\, z\mathbf{k} - \frac{3\alpha V_{xy}(t)}{a^2}[x\mathbf{i} - y\mathbf{j}]\end{aligned} \tag{12}$$

in which

$$\omega_z = \left(\frac{2\alpha q V_T}{ma^2}\right)^{1/2} \tag{13}$$

is the axial or $z$ oscillation frequency. On substitution into eq 1, eq 12 may be analyzed into an equation for axial motion and one for azimuthal motion

$$\ddot{z} + \gamma\dot{z} + \omega_z^2 z = 0 \tag{14}$$

$$\ddot{\boldsymbol{\varrho}} - \omega_c\mathbf{k} \times \dot{\boldsymbol{\varrho}} + \gamma\dot{\boldsymbol{\varrho}} - {}^1/_2\omega_z^2\boldsymbol{\varrho} + \phi_{xy}(t)\,[x\mathbf{i} - y\mathbf{j}] = 0 \tag{15}$$

in which

$$\phi_{xy}(t) = \frac{3q\alpha V_{xy}(t)}{ma^2} \tag{16}$$

and

$$\boldsymbol{\varrho} = x\mathbf{i} + y\mathbf{j} \tag{17}$$

is the radial position vector, and

$$\omega_c = \frac{qB}{m} \tag{18}$$

is the unperturbed ion cyclotron frequency.

It is algebraically convenient to express the azimuthal motion of eq 15 in complex coordinates $(x,iy)$

$$\ddot{\varrho} + i\omega_c\dot{\varrho} + \gamma\dot{\varrho} - {}^1/_2\omega_z^2\varrho + \phi_{xy}(t)\,\varrho^* = 0 \tag{19}$$

in which

$$\varrho = x + iy \tag{20a}$$

$$\varrho^* = x - iy \tag{20b}$$

## D. V-Vector Representation of Equations of Motion for Magnetron/Cyclotron Interconversion

Brown and Gabrielse[29] originally suggested that the above azimuthal motion eq 19 may be further simplified by introduction of two new "V-vector" complex variables, $V^+$ and $V^-$

$$V^+ \equiv V_x^+ + iV_y^+ = \dot{\varrho} - i\omega_-\varrho \tag{21a}$$

$$V^- \equiv V_x^- + iV_y^- = \dot{\varrho} - i\omega_+\varrho \tag{21b}$$

in which

$$V_x^+ = \dot{x} + \omega_- y \tag{22a}$$

$$V_y^+ = \dot{y} - \omega_- x \tag{22b}$$

$$V_x^- = \dot{x} + \omega_+ y \tag{22c}$$

$$V_y^- = \dot{y} - \omega_+ x \tag{22d}$$

$$\omega_\pm \equiv \frac{\omega_c}{2} \pm \sqrt{\frac{\omega_c^2}{4} - \frac{\omega_z^2}{2}} \tag{22e}$$

Here $\omega_c$ is the unperturbed cyclotron frequency, $\omega_+$ is the reduced cyclotron frequency, and $\omega_-$ is the magnetron frequency. $V^+$ and $V^-$ represent the cyclotron and magnetron velocities, including both the orbital motion in the absence of power absorption and the time rate of change of cyclotron and magnetron radius due to power absorption. $V^+$ and $V^-$ may also be thought of as coordinates for cyclotron and magnetron motions treated as independent "normal modes".

The complex position, $\varrho$, and its derivative $(\dot{\varrho})$ may be expressed as functions of $V^+$ and $V^-$

$$\varrho = -\frac{i(V^+ - V^-)}{\omega_+ - \omega_-} \tag{23a}$$

and

$$\varrho = \frac{\omega_+ V^+ - \omega_- V^-}{\omega_+ - \omega_-} \tag{23b}$$

(The quantity, $\omega_+ - \omega_-$, is called the "parametric" frequency.) The azimuthal motion equations may then be rewritten as

$$\frac{dV^+}{dt} + i\omega_+ V^+ + \eta^+ V^+ + i\frac{\Omega(t)}{2}(V^{+*} - V^{-*}) = 0 \tag{24a}$$

$$\frac{dV^-}{dt} + i\omega V^- - \eta^- V^- + i\frac{\Omega(t)}{2}(V^{+*} - V^{-*}) = 0 \tag{24b}$$

in which

$$\eta^+ = \frac{\gamma\omega_+}{\omega_+ - \omega_-} \tag{25a}$$

$$\eta^- = \frac{\gamma\omega_-}{\omega_+ - \omega_-} \tag{25b}$$

and

$$\Omega(t) = \frac{2\phi_{xy}(t)}{\omega_+ - \omega_-} = \frac{6q\alpha V_{xy}(t)}{ma^2(\omega_+ - \omega_-)} \tag{26}$$

and

$$V^{+*} = V_x^+ - iV_y^+ \tag{27a}$$

$$V^{-*} = V_x^- - iV_y^- \tag{27b}$$

There is simple relation between $\Omega(t)$ and the frequency of interconversion between magnetron and cyclotron modes during azimuthal quadrupolar resonant excitation in the absence of collisional damping (see next section). When only the interconversion between magnetron and cyclotron motion is considered, $V^{+*}$ may be dropped from eq 24a and $V^{-*}$ may be dropped from eq 24b, since they rotate twice as fast as $V^+$ and $V^-$, leaving

$$\frac{dV^+}{dt} + i\omega_+ V^+ + \eta^+ V^+ - i\frac{\Omega(t)}{2} V^{-*} = 0 \tag{28a}$$

$$\frac{dV^-}{dt} + i\omega_- V^- - \eta^- V^- + i\frac{\Omega(t)}{2} V^{+*} = 0 \tag{28b}$$

## III. Resonant Azimuthal Quadrupolar Excitation

Solution of the azimuthal ion motion eqs 28 is much simplified when the applied excitation voltage, $V_{xy}(t)$, oscillates at the resonant frequency, $\omega_c = \omega_+ + \omega_-$, of the conversion process:

$$V_{xy}(t) = V_{xy0} \sin \omega_c t \tag{29}$$

$\Omega(t)$ may then be rewritten as

$$\Omega(t) = 2k_0(e^{i\omega_c t} - e^{-i\omega_c t}) \tag{30}$$

in which

$$k_0 = \frac{3q\alpha V_{xy0}}{2ima^2(\omega_+ - \omega_-)} \tag{31}$$

As suggested by Bollen *et al.*[43] we use the following transformation to simplify further eqs 28:

$$V^+(t) = A^+(t)\, e^{-i\omega_+ t} \tag{32a}$$

$$V^-(t) = A^-(t)\, e^{-i\omega_- t} \tag{32b}$$

Equations 32a and 32b may be interpreted as transformations to coordinate frames rotating at the cyclotron and magnetron frequencies, respectively. Substituting eqs 32 into eqs 28, we obtain equations describing the (much slower) motions in the cyclotron and magnetron rotating frames:

$$\frac{dA^+}{dt} = -\eta^+ A^+ - ik_0 A^{-*} \tag{33a}$$

$$\frac{dA^-}{dt} = \eta^- A^- + ik_0 A^{+*} \tag{33b}$$

or, in $x$ and $y$ component equations

$$\frac{dA_x^+}{dt} = -\eta^+ A_x^+ - k_0 A^-{}_y \tag{33c}$$

$$\frac{dA_y^+}{dt} = -\eta^+ A_y^+ - k_0 A_x^- \tag{33d}$$

$$\frac{dA_x^-}{dt} = \eta^- A_x^- + k_0 A_y^+ \tag{33e}$$

$$\frac{dA_y^-}{dt} = \eta^- A_y^- + k_0 A_x^+ \tag{33f}$$

Solution of the four equations is equivalent to a standard eigenvalue problem whose eigenvalues may be obtained from the roots of the characteristic equation

$$\begin{vmatrix} -\eta^+ - \lambda & 0 & 0 & -k_0 \\ 0 & -\eta^+ - \lambda & -k_0 & 0 \\ 0 & k_0 & \eta^- - \lambda & 0 \\ k_0 & 0 & 0 & \eta^- - \lambda \end{vmatrix} = 0 \tag{34}$$

The equation has two degenerate eigenvalues

$$\lambda^{\pm} = \frac{(-\eta^+ + \eta^-)^- + [(\eta^+ + \eta^-)^2 - 4|k_0|^2]^{1/2}}{2} \tag{35}$$

in which $\eta^+$, $\eta^-$, and $k_0$ are defined by eqs 25 and 31, respectively. The solutions to eqs 33 may now be expressed as linear combinations of the eigenfunctions, $e^{\lambda_+ t}$ and $e^{\lambda_- t}$

$$A^+(t) = C_1 e^{\lambda_+ t} + C_2 e^{\lambda_- t} \tag{36a}$$

$$A^-(t) = D_1 e^{\lambda_+ t} + D_2 e^{\lambda_- t} \tag{36b}$$

in which $C_1$, $C_2$, $D_1$, and $D_2$ are constants which depend on the initial conditions for $A^+(t)$ and $A^-(t)$ (or $V^+(t)$ and $V^-(t)$):

$$C_1 = (\lambda^- - \eta^-)\left(\frac{-(\eta^+ + \lambda^+)A^+(0) + k_0 A^-(0)}{(\eta^+ + \lambda^+)(\eta^- - \lambda^-) - |k_0|^2}\right) \tag{37a}$$

$$C_2 = k_0\left(\frac{k_0A^+(0) + (\eta^- - \lambda^-)A^-(0)}{(\eta^+ + \lambda^+)(\eta^- - \lambda^-) - |k_0|^2}\right) \quad (37b)$$

$$D_1 = k_0\left(\frac{(\eta^+ + \lambda^+)A^+(0) + k_0A^-(0)}{(\eta^+ + \lambda^+)(\eta^- - \lambda^-) - |k_0|^2}\right) \quad (37c)$$

$$D_2 = (\eta^+ + \lambda^+)\left(\frac{-k_0A^+(0) + (\eta^- - \lambda^-)A^-(0)}{(\eta^+ + \lambda^+)(\eta^- - \lambda^-) - |k_0|^2}\right) \quad (37d)$$

The final solution for $V^+(t)$ and $V^-(t)$ may then be expressed in the form

$$V^+(t) = C_1e^{(\lambda^+ - i\omega_+)t} + C_2e^{(\lambda^- - i\omega_+)t} \quad (38a)$$

$$V^-(t) = D_1e^{(\lambda^+ - i\omega_-)t} + D_2e^{(\lambda^- - i\omega_-)t} \quad (38b)$$

## A. Relation between V-Vectors and Cyclotron and Magnetron Radius Vectors

Up to this point, we have extensively used the V-vector formulation to derive the equations of ion motion. Although the V-vectors defined in eqs 21 completely describe the ion azimuthal position and velocity at any given instant, it is useful to relate them to the more familiar cyclotron and magnetron radius. We therefore first rigorously define magnetron and cyclotron radius. In the absence of excitation, the position (in complex notation, as usual), $\varrho$, of an ion may be written as the sum of the two independent cyclotron and magnetron components

$$\varrho \equiv x + iy = \varrho_+e^{-i\omega_+t} + \varrho_-e^{-i\omega_-t} \quad (39)$$

in which $\varrho_+$ and $\varrho_-$ are the cyclotron and magnetron radii. The relation between the rotating-frame A-vectors (eqs 36) and the cyclotron and magnetron radii may be found by substituting eqs 32 and eq 23a into eq 39 to give

$$\varrho_+e^{-i\omega_+t} + \varrho_-e^{-i\omega_-t} = -\frac{i(A^+e^{-i\omega_+t} - A^-e^{-i\omega_-t})}{\omega_+ - \omega_-} \quad (40)$$

By comparing the coefficients preceding $e^{-i\omega_+t}$ and $e^{-i\omega_-t}$, we find

$$\varrho_+ = -\frac{iA^+}{\omega_+ - \omega_-} \quad (41a)$$

$$\varrho_- = \frac{iA^-}{\omega_+ - \omega_-} \quad (41b)$$

Finally, from the relation between the rotating-frame A-vectors and the lab-frame V-vectors (eqs 32), we find the relation between the V-vectors and magnetron and cyclotron radius:

$$\varrho_+ = -\frac{iV^+e^{i\omega_+t}}{\omega_+ - \omega_-} \quad (42a)$$

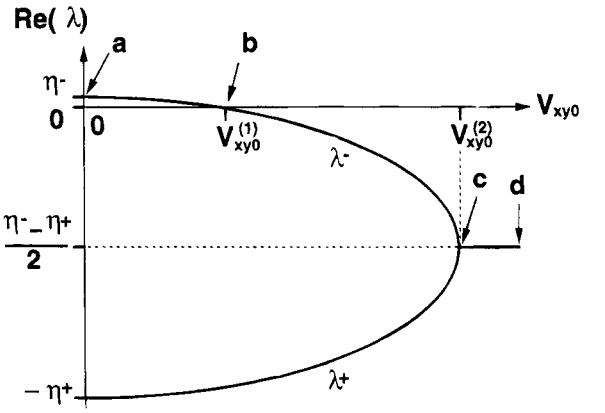


**Figure 5.** Real part of eigenvalues for resonant quadrupolar excitation in the presence of collisional damping. In the region between $a$ and $b$, $\lambda^-$ is positive and $\lambda^+$ is negative, indicating magnetron expansion and cyclotron damping. Between $b$ and $c$, both magnetron and cyclotron motions are damped, but at different rates. If the excitation amplitude is beyond the point $c$, cyclotron and magnetron motions are damped at the same rate and they are interconverted periodically back and forth. (See text.)

$$\varrho_- = \frac{iV^-e^{i\omega_-t}}{\omega_+ - \omega_-} \quad (42b)$$

## B. Ion Trajectory during Resonant Azimuthal Quadrupolar Excitation and/or Collisional Damping

Ion trajectories for resonant azimuthal quadrupolar excitation and/or collisional damping are completely described by the solution (eqs 28) of the azimuthal equation of ion motion and its eigenvalues (eq 35). Figure 5 shows the real part of the eigenvalues as a function of azimuthal quadrupolar excitation amplitude, $V_{xy0}$. We next consider various qualitatively different ion behaviors corresponding to different experimental conditions.

### *1. Collisional Damping, No xy Excitation ($V_{xy0} = 0$)*

In the absence of $xy$ excitation ($k_0 = 0$ on the ordinate axis in Figure 5), the eigenvalues are real, $\lambda^+ = -\eta^+$ and $\lambda^- = \eta^-$. Cyclotron and axial motions behave as damped harmonic oscillators (i.e., negative damping rate constant in eqs 43a and 43c, respectively), whereas magnetron velocity increases exponentially with time (i.e., positive damping rate constant in eq 43b):

$$V^+(t) = V^+(0)e^{-\eta^+t}e^{-i\omega_+t} \quad (43a)$$

$$V^-(t) = V^-(0)e^{\eta^-t}e^{-i\omega_-t} \quad (43b)$$

$$z(t) = z(0)e^{-\gamma t/2}\sin(\omega_zt) \quad (43c)$$

In more familiar terms, we may use eqs 42 to express eqs 43a and 43b in terms of cyclotron and magnetron radii:

$$\varrho_+(t) = -\frac{iV^+e^{i\omega_+t}}{\omega_+ - \omega_-} = -\frac{iV^+(0)}{\omega_+ - \omega_-}e^{-\eta^+t} \quad (43d)$$

$$\varrho_-(t) = \frac{iV^-e^{i\omega_-t}}{\omega_+ - \omega_-} = \frac{iV^-(0)}{\omega_+ - \omega_-}e^{\eta^-t} \quad (43e)$$

The damping rate constants for cyclotron and axial motions are $\eta^+$ $(=(\gamma\omega_+)/(\omega_+ - \omega_-))$ and $\gamma/2$, respectively. The rate constant for increase in magnetron motion is $\eta^-$ $(= (\gamma\omega_-)/(\omega_+ - \omega_-))$. The trajectories of the three motions are shown in Figure 3, along with a graph showing the time evolution of cyclotron radius, magnetron radius, and trapping oscillation amplitude on a common time scale. Note that the cyclotron radius damps about twice as fast, $2\omega_+/(\omega_+ - \omega_-)$, as the trapping oscillation amplitude, and that the cyclotron radius damps much faster, (factor of $\omega_+/\omega_-$), than the magnetron radius grows with time due to ion–neutral collisions. These relative amplitudes account for the efficacy of azimuthal quadrupolar excitation for axialization of ions, because such excitation converts magnetron motion to cyclotron motion, which is then collisionally damped rapidly so that ions end up with very small magnetron radius (i.e., "axialized").

### 2. Azimuthal Quadrupolar Excitation at Frequency $\omega_c$

In this section, the initial axial amplitude and cyclotron radius are taken to be zero. This assumption is justified in actual experiments, because (see Figure 3) cyclotron and axial motion are rapidly cooled to near-zero amplitude by ion–neutral collisions, before azimuthal quadrupolar excitation is applied. Because the exponential growth in magnetron radius is much slower than damping of cyclotron and axial motions, such initial cooling does not result in ion radial diffusive loss.[67]

**a. No Collisional Damping ($\gamma = 0$), Magnetron/Cyclotron Interconvesion.** In the zero-pressure limit (i.e., zero collisional damping), the eigenvalues become

$$\lambda^+ = -i\omega_{beat} \tag{44a}$$

$$\lambda^- = i\omega_{beat} \tag{44b}$$

in which

$$\omega_{beat} \equiv |k_0| = \frac{3q\alpha V_{xy0}}{2ma^2(\omega_+ - \omega_-)} \tag{45}$$

If the initial cyclotron radius is zero, $V^+(0) = 0$, the V-vector may be written

$$V^+(t) = iV^-(0)\sin(\omega_{beat}t)e^{-i\omega_+ t} \tag{46a}$$

$$V^-(t) = V^-(0)\cos(\omega_{beat}t)e^{-i\omega_- t} \tag{46b}$$

or

$$\varrho_+(t) = \frac{V^-(0)}{\omega_+ - \omega_-}\sin(\omega_{beat}t) \tag{46c}$$

$$\varrho_-(t) = \frac{iV^-(0)}{\omega_+ - \omega_-}\cos(\omega_{beat}t) \tag{46d}$$

It is clear that initially pure magnetron motion is converted into pure cyclotron motion after an irradiation period, $t = \pi/(2\omega_{beat})$ and pure cyclotron motion is converted back into pure magnetron motion after an equal additional period (see Figure 6). It is of interest to note that the cyclotron motion and magnetron motions have 90° initial phase difference, even though the initial cyclotron amplitude is zero (see eqs 46c and 46d).

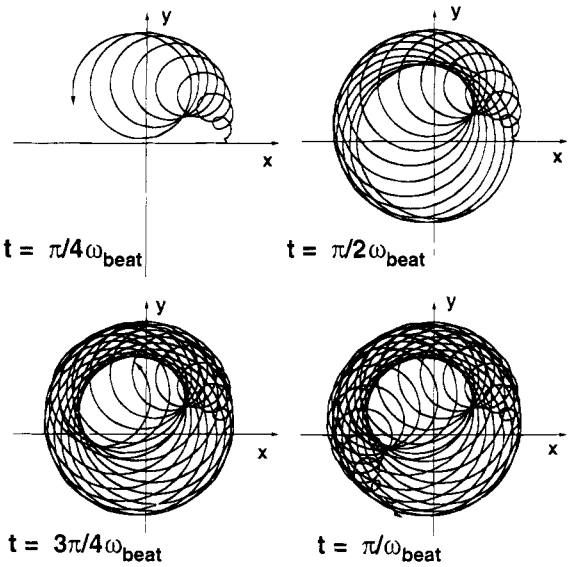


**Figure 6.** Successive stages of ion motion during azimuthal quadrupolar excitation at $\omega_c$, in the absence of collisional damping. Beginning at upper left with pure magnetron motion (zero cyclotron radius), magnetron motion is completely converted to pure cyclotron motion after $\pi/2$ radians of phase at the "beat" frequency (upper right), and eventually back to pure magnetron motion after $\pi$ radians of phase at the "beat" frequency, $\omega_{beat}$. (See text.)

**b. Collisional Damping, Low-Amplitude Azimuthal Quadrupolar Excitation.** When the quadrupolar excitation amplitude is low (i.e., $V_{xy0} < V_{xy0}^{(1)}$ in Figure 5), the eigenvalues, $\lambda^+$ and $\lambda^-$, corresponding to cyclotron and magnetron motion are real and $\lambda^+ < 0$ and $\lambda^- > 0$. Thus, the cyclotron amplitude damps and the magnetron motion expands exponentially with time (Figure 7, upper left). The damping and expansion rates depend on the excitation amplitude, $V_{xy0}$. When

$$\lambda^- = 0 \tag{47}$$

or

$$V_{xy0} = V_{xy0}^{(1)} \equiv \frac{2ma^2\gamma\sqrt{\omega_+\omega_-}}{3q\alpha} \tag{48}$$

the magnetron radius remains constant during quadrupolar irradiation (see Figure 7, upper right). Equation 47 corresponds to the zero-pressure limit, and eq 48 corresponds to a magnetron "confinement" condition for which the collision-induced expansion in magnetron radius is exactly balanced by the magnetron radius damping due to incipient conversion to cyclotron motion (which is in turn rapidly damped by collisions).

**c. Collisional Damping, Intermediate-Amplitude Azimuthal Quadrupolar Excitation.** At higher quadrupolar excitation amplitude, the magnetron radius is also damped by collisions (i.e., $V_{xy0} > V_{xy0}^{(1)}$). The eigenvalues, $\lambda^+$ and $\lambda^-$ are still both real and they are negative (i.e., both cyclotron and magnetron radii are damped by collisions). The absolute value of $\lambda^+$ is smaller than $\eta^+$, indicating that cyclotron motion damps at a slower rate than in the absence of quadrupolar excitation. This situation represents a sort of "critical" damping—

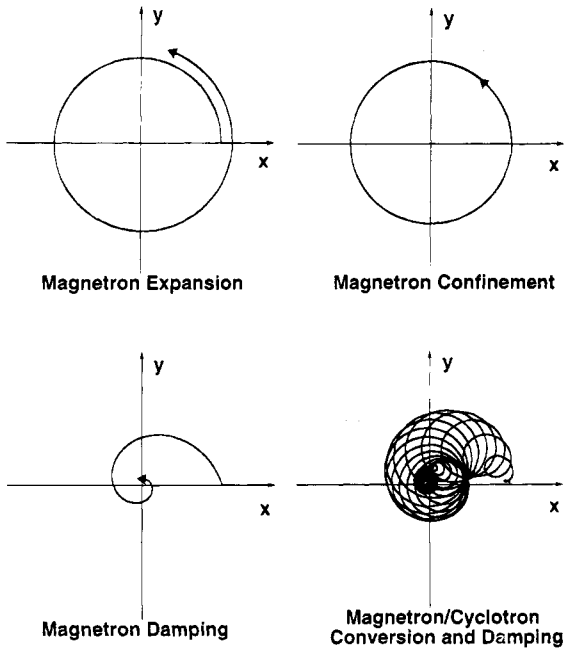


**Figure 7.** Qualitative ion trajectory behavior for each of four different azimuthal quadrupolar excitation amplitudes, for a given collision rate, for ions with zero initial cyclotron radius and nonzero initial magnetron radius. At zero excitation amplitude (upper left), the magnetron radius continues to expand exponentially. At sufficient excitation amplitude (upper right), the magnetron radius is held constant. At even higher excitation amplitude (lower left), the magnetron radius damps exponentially with time, but cyclotron motion never appears. Finally, at very high excitation amplitude (lower right), magnetron and cyclotron radii damp at the same rate and the two motions periodically interconvert. See text for expressions describing the boundaries between these limiting behaviors.

magnetron motion is never converted to cyclotron motion; rather, collisions damp the cyclotron radius to zero faster than magnetron motion can be converted to cyclotron motion. This ion behavior remains qualitatively the same in the range, $V_{xy0}^{(1)} < V_{xy0} < V_{xy0}^{(2)}$, where

$$V_{xy0}^{(2)} \equiv \frac{ma^2\gamma\omega_c}{3q\alpha} \tag{49}$$

corresponding to

$$[(\eta^+ + \eta^-)^2 - 4\,|k_0|^2]^{1/2} = 0 \tag{50}$$

Figure 7 (lower left) shows damping of magnetron motion at the maximal (eq 49) rate $((-\eta^+ + \eta^-)/2)$.

**d. Collisional Damping, high-Amplitude Azimuthal Quadrupolar Excitation.** For quadrupolar excitation amplitude greater than $V_{xy0}^{(2)}$, the imaginary part of the eigenvalues is no longer zero, indicating that magnetron motion is periodically converted to cyclotron motion (and back to magnetron motion). The real parts of $\lambda^+$ and $\lambda^-$ are equal and negative; therefore both cyclotron and magnetron motions are damped at the same rate (Figure 7, lower right). Thus, in ion axialization experiments, it is desirable to apply quadrupolar excitation with an amplitude equal to $V_{xy0}^{(2)}$. At that excitation amplitude, ions are axialized at the maximal rate, and magnetron motion is not converted to cyclotron motion. At lower excitation amplitude, magnetron motion is damped more slowly (if at all), whereas at higher excitation amplitude, magnetron motion is damped, but initial magnetron potential energy is converted into cyclotron kinetic energy, and ions may be lost because of too-large cyclotron radius and/or due to increased cyclotron kinetic energy resulting in collisional activation.

### C. Exact Potential Computation and Ion Trajectory Simulation

All of the theory developed in the proceeding sections is based on assumed pure axial quadrupolar trapping potential and pure azimuthal quadrupole excitation potential. In an actual (e.g., cubic or cylindrical) ICR ion trap, both trapping and excitation potentials deviate significantly from quadrupolar form as ions move away from the center of the trap. Ion trajectories in such nonquadrupolar potentials may not be accurately predicted by the relatively simple analytical solutions presented here. We have therefore developed a numerical method to calculate ICR ion trap potentials with high precision and to simulate ion trajectories subjected to a variety of trapping and excitation conditions.[68,69]

For example, Figure 8 shows two-dimensional isopotential contours in the $xy$ midplane ($z = 0$) for an azimuthal quadrupolar excitation potential applied to a cubic trap, along with isopotential contours for a pure azimuthal quadrupolar potential for comparison. Near the center of the trap, the actual azimuthal quadrupolar excitation potential is well approximated by a pure quadrupolar potential.

Figure 9 shows simulated ion trajectories in a cubic trap subject to static trapping in the absence of collisions or excitation (left), collisional damping in the absence of excitation for zero trapping oscillation amplitude (middle), and axialization produced by quadrupolar excitation in the presence of collisional cooling for zero trapping oscillation amplitude (right). Our simulation algorithm is readily adapted to take into account various nonlinear effects (e.g., Coulomb repulsions between ions) and other experimental conditions (e.g., holes in various electrodes), provides for visualization in real-time video format, and simulates the induced ICR signal generated by an ensemble of many ions.

## *IV. Broad-Band Azimuthal Quadrupolar Excitation*

The theory described in the previous sections shows that ions of a single mass to charge (m/z) ratio (i.e., a single $\omega_c$ value) may be axialized by azimuthal quadrupolar excitation at the unperturbed cyclotron frequency, $\omega_c$. For analytical mass spectra, it is more desirable to axialize ions over a broad m/z range. The extension of single-frequency or resonant axialization to broad-band procedures requires understanding of ion motion response to broad-band azimuthal quadrupolar excitation. Surprisingly, the magnetron-to-cyclotron interconversion is *not* a linear process. In the following sections, we first establish a connection between magnetron/cyclotron interconversion and an excitation process in a quantum mechanical two energy level system and then discuss a practical method to achieve broad-band axialization based on linear response theory.

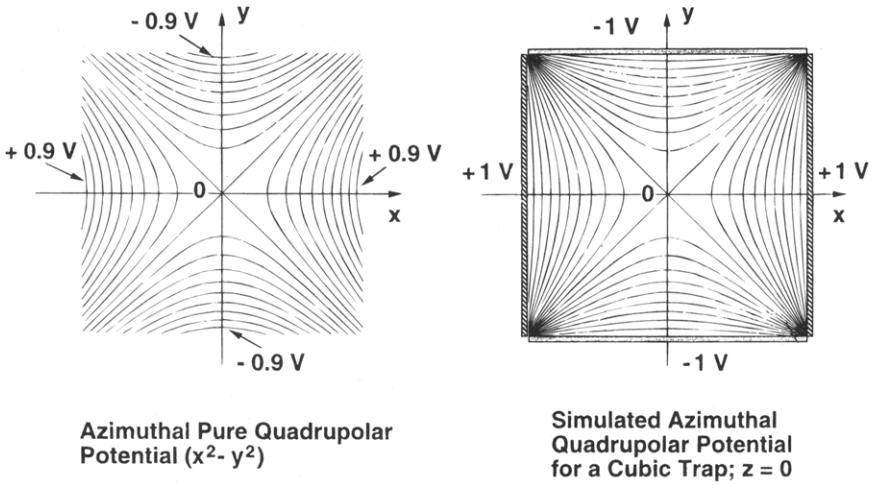


**Figure 8.** Two-dimensional isopotential contours of a perfect azimuthal quadrupolar excitation potential (left) and the numerically computed potential at the midplane of a cubic ICR ion trap (right). Near the center of the trap, the cubic trap potential closely approximates the pure quadrupolar potential.

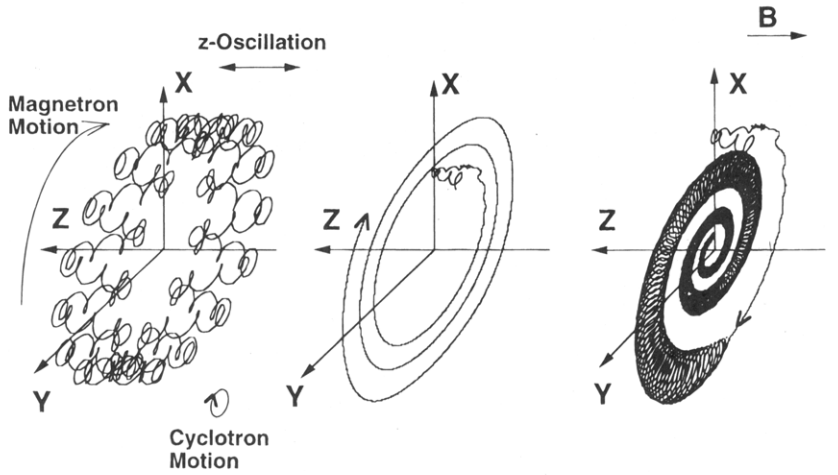


**Figure 9.** Numerical simulation of ion trajectories in a cubic ICR ion trap, for an ion of m/z 1000; initial position, (0.3$a$, 0, 0.1$a$); initial kinetic energy, 0.065 eV (equivalent to 500 K temperature); and 2 V trapping voltage. Left: projection of three-dimensional simultaneous periodic cyclotron, magnetron, and axial motions in the absence of collisional damping and electric excitation. Addition of collisions represented as friction with damping constant, 10000 $s^{-1}$ (middle) quickly damps the cyclotron and axial motions, while the magnetron radius grows exponentially at a slower rate. Once the cyclotron and axial motions are nearly completely damped (right), azimuthal quadrupolar excitation at the unperturbed cyclotron frequency ($2V_{p-p}$) periodically interconverts magnetron and cyclotron motion and damps the cyclotron radius to bring ions back to the center of the trap after a few magnetron cycles. This simulation provides an accurate picture of what happens in actual experiments. (Reprinted from ref 68. Copyright 1994 Elsevier.)

## A. Relation of Magnetron/Cyclotron Conversion to a Quantum Mechanical Two-Level Spin System

In the absence of collisional damping ($\gamma \approx 0$), eq 28 simplifies to

$$\frac{dV^+}{dt} + i\omega_+ V^+ - i\frac{\Omega(t)}{2} V^{-*} = 0 \qquad (51a)$$

$$\frac{dV^-}{dt} + i\omega_- V^- + i\frac{\Omega(t)}{2} V^{+*} = 0 \qquad (51b)$$

(For single-frequency resonant excitation, $\Omega(t)$ is given by eq 30.) It can be proved[50] that

$$|V^+|^2 + |V^-|^2 = C \qquad (52)$$

in which $C$ is a constant determined by the initial conditions. Equation 52 is formally analogous to the equation for a circle: $x^2 + y^2 = r_0^2$. Therefore, the conservation of $|V^+|^2 + |V^-|^2$ suggests the following transformation for the normalized V-vectors:

$$V^+ = \sin(\theta/2)\, e^{i\psi_+} \qquad (53a)$$

$$V^- = \cos(\theta/2)\, e^{i\psi_-} \qquad (53b)$$

in which $\psi_+$ and $\psi_-$ are the respective phases of $V^+$ and $V^-$. The amplitudes of $V^+$ and $V^-$ are $\sin(\theta/2)$ and $\cos(\theta/2)$. (For single-frequency resonant excitation, $\theta/2 = \omega_{beat}t$.) In eqs 53, it is understood that $0 \le \theta \le \pi$, so that the V-vector amplitudes are positive. Equations 51 may be combined to yield

$$\left(\frac{d\theta}{dt}\cos\theta + i\left(\frac{d\phi}{dt} - \omega\right)\sin\theta\right) e^{i\phi} = i\cos\theta\,\Omega(t) \qquad (54)$$

in which

$$\phi = \psi_+ + \psi_- \qquad (55a)$$

$$\omega = \omega_+ + \omega_- \qquad (55b)$$

Guan has pointed out that eq 54 is formally identical to the Bloch equations which describe the evolution of a quantum mechanical two-level system (e.g., a particle of spin one-half in a static magnetic field) in spherical coordinates.[70] In the present case, $\omega$ is positive in sign because the applied static magnetic

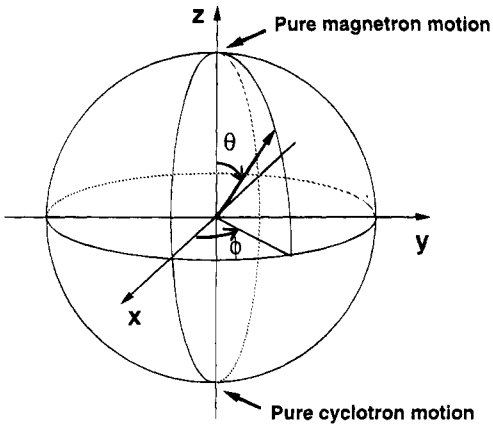


**Figure 10.** Magnetron-to-cyclotron conversion, in a three-dimensional vector display modeled after a Bloch equation representation of magnetization trajectory during resonant excitation of a two-level quantum mechanical spin-$^1/_2$ system in the absence of relaxation. The "north pole" (analogous to equilibrium magnetization) represents pure magnetron motion, and the "south pole" (inverted magnetization) represents the pure cyclotron motion. Azimuthal quadrupolar excitation for one-fourth cycle of the "beat" frequency (see text) has the effect of a "$\pi$ pulse", and converts magnetron motion completely into cyclotron motion. (See eq 53.)

field is defined to lie along the negative $z$ axis, leading to counterclockwise rotation of $\omega_+$ and $\omega_-$.

Equations 54 and 55 imply that a complete conversion from magnetron motion to cyclotron motion corresponds to an excitation process that takes the "flip angle", $\theta$, from 0 to $\pi$. The analog between magnetron/cyclotron interconversion and excitation of a two-level spin system allows one to display the conversion process by the familiar three-dimensional vector model for dipolar excitation of an equilibrium magnetic moment (see Figure 10). From careful study of the properties of eq 54, an algorithm for generating optimal excitation pulses has been proposed.[70] The use of the algorithm for producing a $\pi/2$ notch excitation pulse has been demonstrated. For the purpose of complete conversion of magnetron and cyclotron motion, it is necessary to generate $\pi$ pulses. Thus far, there is no general method for generating an inversion pulse with an arbitrary broad-band magnitude-vs-frequency profile; however, considerable progress has been made.[71] Although the hyperbolic secant pulse for inversion over a range of resonance frequencies is the only one whose response can be expressed analytically,[72] several other pulse shapes can achieve population inversion.[73] A more general approach for generating a (nonselective) adiabatic rapid passage inversion pulse has been proposed by Pines and co-workers.[74]

Once magnetron motion has been completely converted to cyclotron motion, collisional damping of the cyclotron motion axializes the ions. Mass selectivity of axialization depends on the frequency selectivity of the quadrupolar excitation and on the efficiency of collisional damping.

## B. Conservation of Ion Cloud Dimensions

An important consequence of eq 52 is that *the radius of the ion cloud is not changed by an arbitrary excitation which completely converts magnetron motion to cyclotron motion*. For example, suppose that the ion initial cyclotron radius is zero and the initial magnetron radius is nonzero ($V^+(0) = 0$, $V^-(0) = V^-_{initial}$), and that the excitation completely converts magnetron motion to cyclotron motion after a time period, $T$ ($V^+(T) = V^+_{final}$, $V^-(T) = 0$). According to eqs 42, the radius of the ion cloud is described by the radius of magnetron motion before excitation and by the cyclotron radius after excitation:

$$\varrho_{-,initial} = \frac{|V^-_{initial}|}{\omega_+ - \omega_-} \tag{56a}$$

and

$$\varrho_{+,final} = \frac{|V^+_{final}|}{\omega_+ - \omega_-} \tag{56b}$$

From eqs 46, we have

$$|V^+_{final}| = |V^-_{initial}| \tag{57}$$

Therefore, the final radius of the ion cloud ($\varrho_{final}$) is equal to its initial value

$$\varrho_{+,final} = \varrho_{-,initial.} \tag{58}$$

## C. Phase Conservation of Individual V-Vectors

Equation 54 describes time evolution of the amplitudes of $V^+(t)$ and $V^-(t)$ and the combined phase, $\phi = \psi_+ + \psi_-$, in which $\psi_+$ is the phase of cyclotron motion and $\psi_-$ is the phase of magnetron motion. However, the phases of individual V-vectors are not defined in the equation. Unlike the two-level spin system, for which the equilibrium magnetization (zero flip angle) has no defined phase, the magnetron/cyclotron system always has a definite phase, ranging from zero phase for pure magnetron motion to $\pi$ radians for pure cyclotron motion. Fortunately, for the purpose of ion axialization, the phase is irrelevant because the magnetron and cyclotron radii during magnetron/cyclotron interconversion by azimuthal quadrupolar excitation do not depend on the absolute or relative phases of the two motions.

The time evolution of cyclotron and magnetron phases during resonant azimuthal quadrupolar excitation can be rendered experimentally observable by use of an off-center ICR ion trap to create coherent magnetron motion.[75] Magnetron-to-cyclotron interconversion is ordinarily not directly detectable, because ions are usually distributed with random magnetron phase. However, by forming ions with an off-axis electron beam whose duration is short compared to one magnetron cycle, we can produce coherent magnetron motion, which may then be converted to coherent cyclotron motion for detection, as shown in Figure 11. In that figure, two ion packets differing by 180° in initial magnetron phase were created to demonstrate quadrupolar detection as well as quadrupolar magnetron-to-cyclotron conversion. Note that the cyclotron phase *difference* between the two

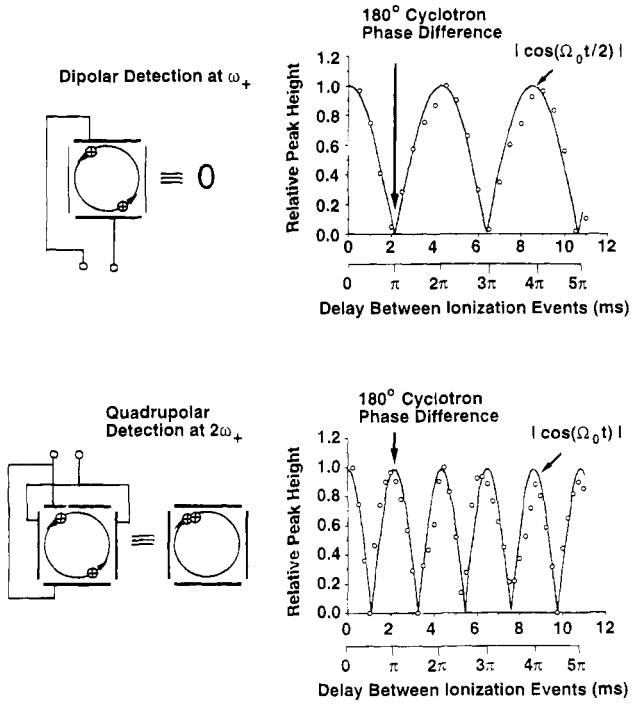


**Figure 11.** Dipolar detection at frequency, $\nu_+$ (top) and quadrupolar detection at frequency, $2\nu_+$ (bottom), following quadrupolar complete magnetron-to-cyclotron conversion of two ion packets whose initial magnetron phases are determined by the delay between the two short electron beam pulses that created the two packets. Ion packets with initial magnetron phase difference of $\pi$ radians (leading to final cyclotron phase difference of $\pi$ radians) give zero dipole and maximal quadrupole signals. Experimental data (electron beam, 500−1750 $\mu$A, −20 eV energy, and 250 $\mu$s duration) are shown as open circles, in excellent agreement with theoretical solid curves based on eq 45. (Reprinted from ref 75. Copyright 1994 American Institute of Physics.)

ion packets after magnetron-to-cyclotron conversion is the same as the initial magnetron phase *difference* between the two ion packets before conversion. The reader is referred to Chen *et al.* for more details.[75]

Most generally, we now show how the *absolute* cyclotron phase of an individual ion packet following magnetron-to-cyclotron conversion is related to the *absolute* magnetron phase before conversion, for an arbitrary excitation waveform. Although eqs 51 completely determine the ion trajectories, it is more convenient to express the V-vectors in terms of the flip angle, $\theta(t)$, and the magnetron and cyclotron phases, $\psi_-(t)$ and $\psi_+(t)$. By solving the Bloch equations in the absence of relaxation, eq 54, we may obtain $\theta(t)$ and $\phi(t)$, from which the time evolution of the desired magnetron and cyclotron phases, $\psi_-(t)$ and $\psi_+(t)$, may be obtained by substituting eqs 54 into eqs 51 individually, and then integrating with respect to time:

$$\psi_-(t) = \frac{1}{2}\int_0^t ([\Omega(\tau)e^{-i\phi(\tau)} - i\theta(\tau)]\tan(\theta(\tau)/2))\,d\tau + \omega_- t + \psi_-(0) \quad (59)$$

and

$$\psi_+(t) = \phi(t) - \psi_-(t) \quad (60)$$

For example, in the simplest case of resonant single-frequency excitation at $\omega_c$, the integral in eq 59 vanishes: the magnetron phase during azimuthal quadrupolar excitation thus evolves as it would in absence of such excitation, namely, $\psi_-(t) = \psi_-(0) + \omega_- t$, and the cyclotron phase evolves at the reduced cyclotron frequency, $\psi_+(t) = \psi_+(0) + \omega_+ t$. Thus, the magnetron and cyclotron *radii* vary sinusoidally during azimuthal quadrupolar excitation, but their respective *phases* evolve unaffected by that excitation.

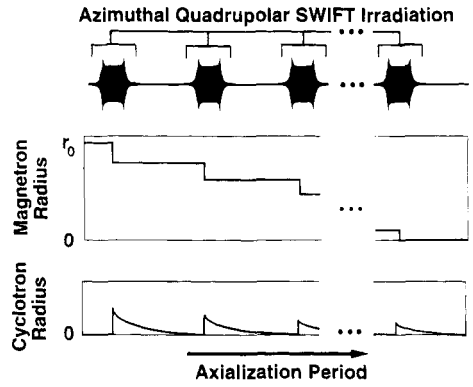


**Figure 12.** Broad-band axialization procedure. A train of azimuthal quadrupolar SWIFT excitations, each of amplitude corresponding to a small "tip angle", $\theta$, in Figure 10, reduces magnetron radii of ions stepwise. Each step converts only a fraction of magnetron radius to cyclotron radius and the cyclotron radius damps nearly to zero before the next repetition. After many such stages, the large initial magnetron radius is reduced to zero. (Reprinted from ref 51. Copyright 1994 American Institute of Physics.)

## D. Broad-Band Axialization by Repeated SWIFT Azimuthal Quadrupolar Excitation

Theoretically, ion axialization over a broad m/z range can be accomplished by the procedure developed in the previous section in which magnetron motion of ions in the range of interest is completely converted to cyclotron motion by a broad-band "$\pi$" pulse. The cyclotron motion is then cooled by collisional damping. As mentioned earlier, shaped pulses to produce highly selective broad-band excitation are not fully understood analytically and no single shaped-pulse method is widely applicable. In ICR, there is the additional problem that the excitation potential is far from pure azimuthal quadrupolar except near the trap center. For all of these reasons, high-amplitude single-event azimuthal quadrupolar excitation has not been successful in producing highly selective magnetron-to-cyclotron conversion over a wide m/z range.

However, suppose that ions have near-zero initial cyclotron and axial motional amplitudes, as a result of collisional cooling before any axialization process. If the azimuthal quadrupolar excitation is sufficiently low in amplitude, then the corresponding magnetron-to-cyclotron conversion process is linear, just as magnetic resonance low-amplitude excitation is linear in the limit of sufficiently small ($\sin\theta \approx \theta$) "tip angle". We may therefore apply a train of low-amplitude successive identical stored waveform inverse Fourier transform (SWIFT) excitations[51] (Figure 12, top), in azimuthal quadrupolar mode, to ions in the presence of a buffer gas. The stored waveform

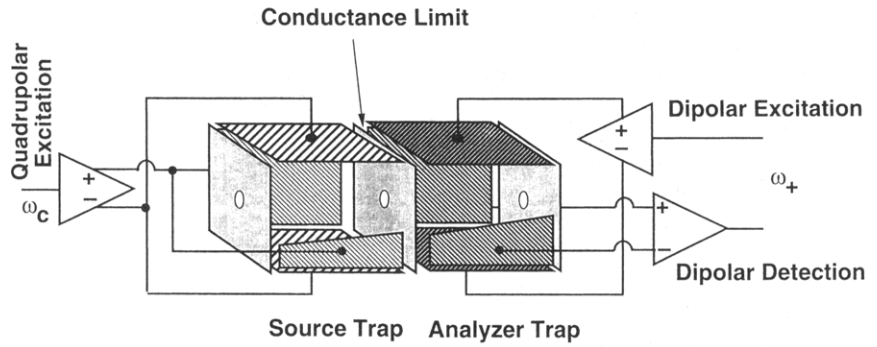


**Figure 13.** Trap configuration for quadrupolar excitation (left) and conventional dipolar excitation (right). In the present experiments, ions are axialized in the presence of buffer gas in the source trap (left) and then passed to the analyzer trap (right) for conventional high-resolution dipolar excitation/detection at low pressure.

is generated by inverse Fourier transform of a desired magnitude–mode excitation spectrum with appropriate phase modulation.[76,77] Each SWIFT irradiation converts a fraction of the magnetron motional amplitude into cyclotron motional amplitude (Figure 12, middle); during the interval between SWIFT excitations, the cyclotron motion quickly damps to near-zero radius (Figure 12, bottom), and the magnetron radius expands only slightly (see the previous section). The process is then repeated, thereby successively reducing the magnetron radius stepwise to zero, and leaving the ions well localized near the center of the trap. Because the magnetron radius is reduced by only a few per cent by any one SWIFT irradiation, the azimuthal quadrupolar excitation process becomes linear,[70] justifying the use of SWIFT excitation, as we shall show below.

## V. Applications for Ion Axialization

For optimal ICR detection, ions should initially possess zero kinetic energy and be located near the center of the trap. After excitation of cyclotron motion, ions have a relatively high velocity; thus, detection should be conducted at low pressure in order to avoid collisional damping of the cyclotron motion.[78] As discussed in the previous sections, ion cyclotron and axial motions can be damped effectively by ion–neutral collisions, and magnetron radius can be reduced by azimuthal quadrupolar excitation in the presence of collisional damping. Unfortunately, in order to reduce the initial ion kinetic energy and localize ions to the center of the trap, one must carry out cooling and axialization procedures at relatively high collision gas pressure, which would appear to be incompatible with high mass-resolving power by conventional FT-ICR excite/detect procedures.

However, ion axialization and ion detection need not take place at the same location and/or at the same time. An obvious solution is to axialize ions at high pressure in a first ICR ion trap, and then transport them to a second spatially separated trap at lower pressure for excitation/detection. Alternatively, a buffer gas may be pulsed into the trap to provide for collisional damping during the axialization process, and then pumped away before excitation/detection in the same trap. Both methods are in use.

For the first method, we used a dual-trap instrument,[45] in which ions were axialized at an argon pressure of $\sim 5 \times 10^{-7}$ Torr in a source trap for 10–30 s and then transferred through a conductance limit to an analyzer trap for high-resolution detection. A schematic wiring diagram for producing azimuthal quadrupolar excitation in the source trap and carrying out dipolar excitation/dipolar detection in the analyzer trap is illustrated in Figure 13. The second method has been demonstrated by Speir *et al.* in a single-trap instrument for improvement of ion remeasurement efficiency,[47] as discussed below. Finally, we have also developed a multiply pulsed collision gas technique for ion axialization in a dual trap for further improving mass-resolving power of laser-desorbed ions.[48]

Very rapid progress has been made in the application of ion axialization since it was introduced into the field of FT-ICR/MS in 1991. We conclude this review with a survey of extensions and applications.

### A. Prolonged and Efficient Ion Trapping at High-Collision Gas Pressure

An important feature of the ion axialization technique is its ability to trap ions at high neutral gas pressure for a long time period. Ions generated by a variety of ionization methods possess high kinetic and internal energy. However, a wide distribution in ion kinetic energy is undesirable for ion detection in any mass analyzer, including ICR. For example, for high-resolution mass analysis in a sector mass spectrometer, ion kinetic energy is first selected by an energy analyzer before ions are sent to the mass analyzer. Similarly, in time-of-flight instruments, ions with different kinetic energy spread out in space during their flight to the detector but may be refocused by a reflectron.

A claimed advantage of a quadrupolar ion trap (QIT) mass spectrometer is the possibility of collisional cooling of ions due to its high operating pressure ($\sim 10^{-3}$ Torr buffer gas pressure). In a QIT, a high-frequency, high-amplitude rf driving voltage applied to the ring electrode of the trap generates an effective "pseudopotential" in which ions are trapped. The pseudopotential has an effective minimum at the center of the trap. Collisions with neutrals establish a thermal "equilibrium" and ion kinetic energy may be reduced to near thermal energy.[79]

An ICR ion trap has a "saddle-point" electrostatic potential which confines ions axially, but pushes ions radially outward (see Figure 1). In the absence of ion–neutral collisions, the magnetic field confines ions radially, because the ions have no way to convert their electrostatic radial potential energy into kinetic

energy. However, ion–neutral collisions allow ions to "roll down" the magnetron potential hill and expand radially outward until they are lost from the trap. Rempel and Gross have applied an rf trapping method to trap ions at high pressure in an ICR ion trap.[80] The rf driving voltage forms an azimuthal psuedopotential that confines the ions from escaping from the trap. Although trapping of ions at high-collision gas pressure is achieved (over a limited m/z range), the high driving voltage amplitude may excite ions whenever they are not at the center of the trap.

In ion axialization experiments, ions in any region of the trap are brought back to the center of the trap by application of low amplitude azimuthal quadrupolar excitation voltage on the electrodes parallel to the magnetic field. For example, at an argon pressure of $1 \times 10^{-5}$ Torr, a thermal ion of m/z 1000 (hard-sphere model) collides about 400 times per second with Ar atoms. At 3 T, in a cubic trap of 5 cm trap edge length, with 2 V dc applied to each of the two trapping plates, the voltage required to confine the magnetron expansion is $V_{xy0}^{(1)} \approx 0.02$ V according to eq 53, and the voltage to achieve the maximum axialization rate is $V_{xy0}^{(2)} \approx 0.2$ V, based on eq 54. Within the voltage range, $V_{xy0}^{(1)} < V_{xy0} < V_{xy0}^{(2)}$, ion cyclotron radius remains near zero (cooled before axialization) and ions possess mainly potential (magnetron) energy. The speed of an ion at 1 cm magnetron radius is about 8 m/s (compared to thermal speed of ~70 m/s for an ion of m/z 1000)—the kinetic energy of magnetron motion may thus be neglected.

With the axialization method, ions may be trapped at a high collision gas pressure for a prolonged period allowing a large number of ion–neutral collisions. In an early experiment, benzene molecular ions were trapped for more than 20 s at $2 \times 10^{-5}$ Torr of Ar (i.e., ~5000 ion–neutral collisions).[45] The observed decrease in ion signal may be due to proton transfer from the axialized molecular ions to neutrals present in the trap. Figure 14 shows a more recent example, in which ions produced by ND:YAG laser desorption of a rhodamine 6G sample possess a radial motional component too large to allow transfer from the source to the analyzer compartment of the ion trap (Figure 14, second spectrum).[46] Selective ion axialization can effectively bring to the center axis of the trap only the protonated molecules ($[M + H]^+$), which may then be transferred to the analyzer trap for detection (Figure 14, third spectrum). In fact, the ions may be trapped in the source trap for 500 s at $\sim 7 \times 10^{-7}$ Torr of Ar pressure, or >10000 collisions (Figure 14, bottom spectrum). The observed loss of ion signal is possibly due to proton transfer from the pseudomolecular ions to neutrals in the source trap. *The long trapping period allows very slow ion–molecule reactions to be observed. Also, it is possible to cool ion internal and kinetic energies to thermal temperature and therefore avoid unimolecular decomposition due to high-energy deposition during ionization processes.*

Trapping efficiency is clearly enhanced by quadrupolar excitation/collisional cooling (see next section) because ion kinetic energy after ion formation, partitioned into cyclotron, axial, and magnetron motions upon entry into the trap, is effectively removed.

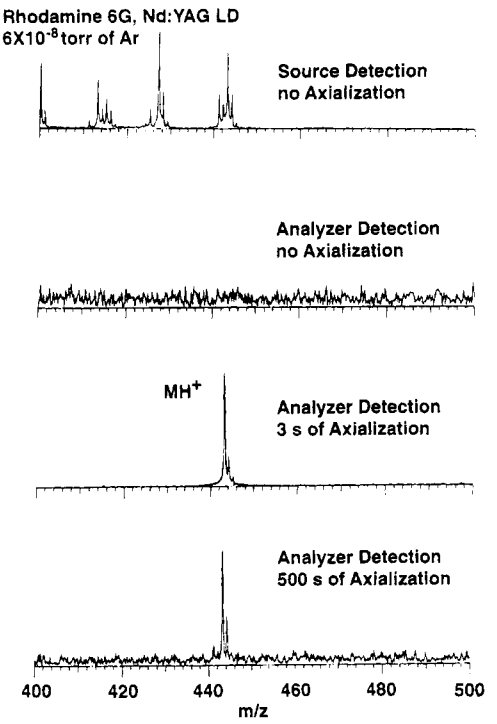


**Figure 14.** Extended trapping by axialization of laser-desorbed rhodamine 6G protonated ions initially present in the source trap of Figure 12. The top spectrum shows detection in the source trap without axialization; second from top, detection in the analyzer trap (because of their large initial magnetron radius following laser desorption/ionization, ions cannot be transferred to the analyzer trap, and no ICR signal is seen); third from top, protonated molecular ions subjected to 3 s of axialization at $5 \times 10^{-7}$ Torr of argon may then be selectively transferred to the analyzer for detection; bottom, ions axialized at $5 \times 10^{-7}$ Torr of argon for 500 s in the source trap (>10000 collisions) are still available for transfer to the analyzer trap for detection. (Reprinted from ref 46. Copyright 1993 American Chemical Society.)

Axialization should therefore prove very useful in extending the m/z range of laser-desorbed ions detectable by FT-ICR/MS. High ion kinetic energy following the desorption event limits the highest observable m/z, because ions of high kinetic energy have large cyclotron radii.[81] With our recently introduced thin gold film-assisted laser desorption/ionization technique,[82] we have been able to trap efficiently peptide ions up to m/z ~2000 after axialization, even though the signal for the same ions without axialization was almost undetectable (Figure 15).

## B. Enhanced Mass-Resolving Power

Because ions can be cooled and axialized in the source trap and detected at a much lower pressure in the analyzer trap, high mass-resolving power may be achieved. Figure 16 shows FT-ICR mass spectra of pseudomolecular ions of rhodamine 6G. When detected in the source trap at a base pressure of $8 \times 10^{-8}$ Torr, the mass-resolving power, $m/\Delta m$ (in which $\Delta m$ is the full peak width at half height) is only ~2400. Admission of Ar gas to a pressure of $1.2 \times 10^{-7}$ Torr increases the mass-resolving power to ~12000 despite the higher pressure (corresponding to faster damping of the cyclotron motion). The increased mass-resolving power is likely due to the

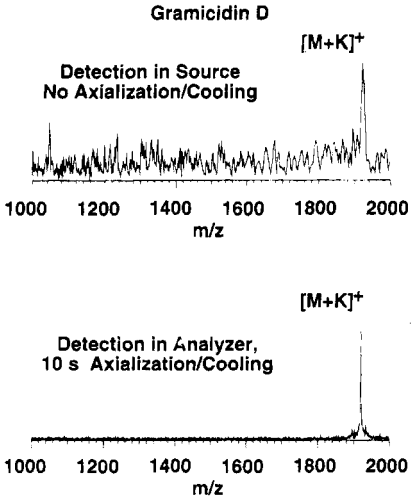


**Figure 15.** Signal-to-noise ratio enhancement by axialization. Top: Gramicidin D quasimolecular ions, $[M + K]^+$, generated by laser desorption/ionization are barely detectable by conventional dipolar excitation/detection in the source trap with the conventional source trap excite/detect procedure. Bottom: Signal-to-noise ratio is vastly improved by 10 s of axialization before transfer to the analyzer trap for dipolar excitation/detection. Reprinted from ref 82. Copyright 1993 American Chemical Society.)

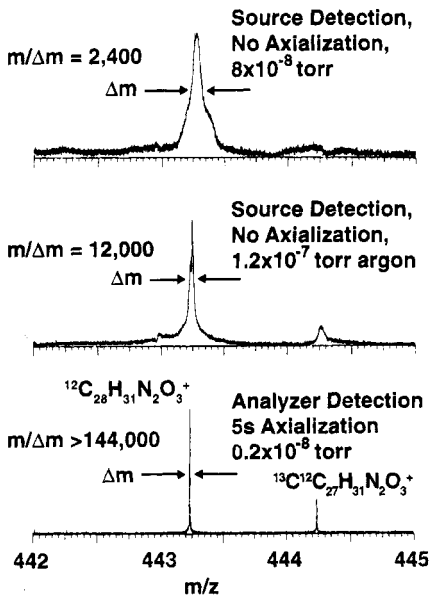


**Figure 16.** Effect of buffer gas collisions with or without azimuthal quadrupolar excitation. Top: Detection of rhodamine 6G protonated molecular ions immediately after laser desorption/ionization from a sample-coated stainless steel plate yields poor mass-resolving power and low signal-to-noise ratio in the source trap. Middle: Addition of $1.2 \times 10^{-7}$ Torr of Ar buffer gas improves mass-resolving power by a factor of ~4.5, by collisional cooling. Bottom: Much higher resolving power (and thus higher signal-to-noise ratio as well) is obtained by azimuthal quadrupolar excitation in the presence of $1.2 \times 10^{-7}$ Torr of argon in the source trap followed by transfer to the analyzer trap for dipolar excitation/detection. (Reprinted from ref 46. Copyright 1993 American Chemcial Society.)

collisional cooling of ion initial kinetic energy prior to excitation/detection. Because damping of cyclotron and axial motions is much faster than magnetron expansion, collisional cooling for a short period (~0.5 s, without axialization) removes ion kinetic energy without causing significant ion cloud radial expansion. The collisionally cooled ions in Figure 16

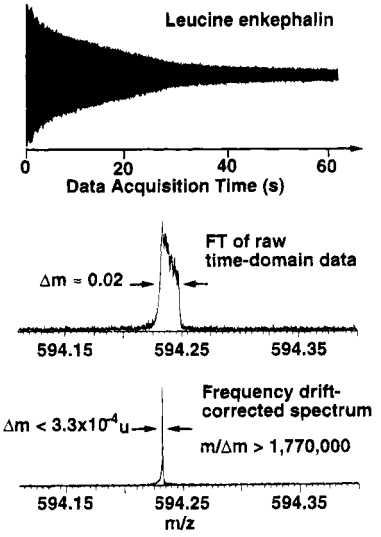


**Figure 17.** Multiply-pulsed collision gas axialization with frequency drift correction for ultrahigh-resolution detection. Top: The time-domain ICR signal from laser-desorbed leucine enkephalin lasts for more than a minute. Middle: Space charge leads to an inhomogeneously broad FT-ICR mass spectrum, due to ICR frequency drift during detection. Bottom: Digital heterodyne frequency drift correction yields an ultrahigh-resolution FT-ICR mass spectrum. This mass spectrum reprresents the highest resolution yet reported for a laser-desorbed peptide. (Reprinted from ref 48. Copyright 1993 Heyden + Son Ltd.)

(middle) are therefore localized in a region of more homogeneous magnetic and electric field during excitation and detection; consequently, inhomogeneous spectral broadening is reduced. However, due to the high pressure in the source trap, the time-domain ICR signal damps too quickly to allow ultrahigh mass-resolving power. If ions are axialized for 5 s, the cooled ions may then be transferred to the analyzer trap where the pressure is about 2 orders of magnitude lower—they may be detected at much higher mass-resolving power (~144000).[46]

Clearly it is desirable to maintain the analyzer trap at the lowest pressure possible to achieve high mass-resolving power during detection. Axialization compresses an ion cloud to very small radial dispersion and should therefore allow for use of a conductance limit smaller than the ~2 mm diameter in our current instrument, to provide a larger pressure difference between the two ion traps. The analyzer trap pressure may be lowered even further by use of pulsed collision gas into the source trap for axialization. In this way, it is possible to obtain a long-lasting transient ICR signal: >60 s for potassiated leucine enkephalin (Figure 17, top). According to the collisional damping model, the predicted mass-resolving power of the signal is $>10^6$. However, the spectrum obtained by direct Fourier transformation of the time-domain ICR signal shows a mass-resolving power of "only" ~297000 (Figure 17, middle), due to slow drift in cyclotron frequency during detection. For laser-desorbed potassiated leucine enkephalin ions, we have observed a large downward frequency drift (corresponding to ~2 m/z) during data acquisition after axialized ions have been transferred to the analyzer trap.

In order to eliminate the frequency drift effect from a spectrum, we devised a deconvolution method based on digital quadrature heterodyning.[49] In general, a

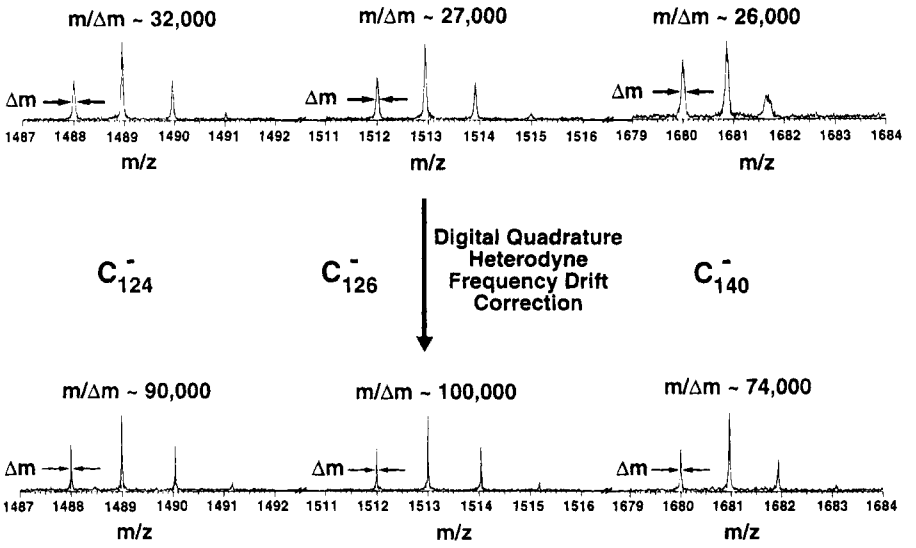


**Figure 18.** Demonstration that digital heterodyne frequency drift correction based on frequency drift of fullerene anions ions of one m/z value also corrects for frequency drift of ions of other m/z values. Thus, mass-resolving power may be enhanced over a wide m/z range with no additional effort.

real time-domain signal may be converted into a complex form whose real and imaginary parts are obtained by multiplication of the original signal with a cosine and sine functions at a reference frequency. The frequency drift in the complex time-domain signal may then be expressed as a phase factor which may be eliminated from the signal. The frequency drift function is obtained by segmenting the original time-domain signal, Fourier transforming each of the successive segments, and polynomial fitting a plot of frequency vs time during the acquisition period. Time integration then yields the instantaneous phase of the detected frequency drifted signal.[49] With this method, order-of-magnitude improvement in mass-resolving power for laser-desorbed potassiated leucine enkephalin could be achieved (Figure 17, bottom). *The mass spectrum in Figure 17 (bottom) represents the highest mass-resolving power obtained to date for a laser-desorbed organic compound.* Finally, it is encouraging to note that the technique also removes frequency drifts from peaks other than the one yielding the correction coefficients. Thus, we also obtained improvement in mass-resolving power for several carbon-13 isotopic peaks of potassiated gramicidin S[49] and for fullerene anions throughout a range, $1400 \leq m/z \leq 1700$ (Figure 18), even though only a single peak in the spectra was selected to construct the frequency drifted phase function.

## C. Mass-Selective Axialization

The ion axialization method is inherently mass selective. For single-frequency azimuthal quadrupolar excitation, only ions resonant to the excitation (i.e., excitation frequency equal to the unperturbed cyclotron frequency) will be axialized. This mass selectivity was noted for low-mass (high-frequency) ions in the first ion axialization experiments performed with FT-ICR detection.[45] The high degree of ion mass selectivity has been extended to high-mass (low-frequency) ions, i.e., selection of $^{12}C_{84}^-$ from a mixture of fullerene anions, with no contamination by $^{12}C_{84-n}$ $^{13}C_n^-$.[46]

Another illustration of the selectivity of the axialization process at high mass is shown in Figure 19.

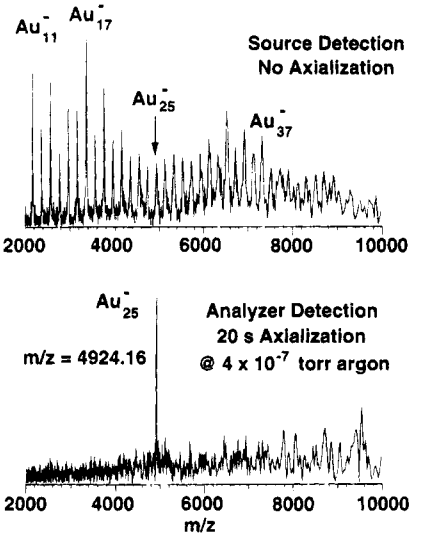


**Figure 19.** Axialization for high-resolution mass selectivity. A minor component, $Au_{25}^-$, from a mixture of gold cluster anions generated by a Nd:YAG laser pulse from a thin gold film (top) may be selectively axialized and transferred to the analyzer trap for detection (bottom). Such experiments make possible improved parent ion selectivity for MS/MS.

Laser desorption of a gold film coated on a glass plate yields a wide distribution of gold cluster anions (Figure 19, top). The gold cluster $Au_{25}^-$ may be selectively axialized from the $Au_n^-$ mixture by application of quadrupolar excitation in an Ar atmosphere ($4 \times 10^{-7}$ Torr) followed by subsequent transfer to the analyzer trap for excitation and detection (Figure 19, bottom).

For analytical purposes, axialization of ions over a broad m/z range is highly desirable and (as discussed in section IV) may be achieved by either of two recently developed methods. In the first method,[50] magnetron motion of ions in a broad m/z range is completely converted to cyclotron motion by a "$\pi$ pulse" and axialization of those ions results from collisional damping of the cyclotron motion. We have produced complete conversion over a wide m/z range by use of an adiabatic rapid passage pulse.[50] However, as expected, mass selectivity is limited. The

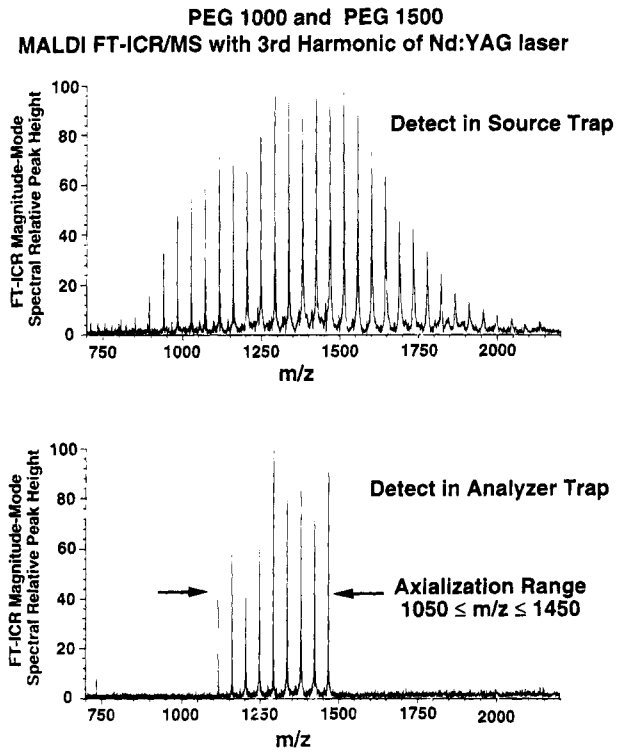


**Figure 20.** Broad-band mass-selective axialization of poly(ethylene glycol) ions. The spectrum shows top matrix-assisted laser desorption/ionization (355 nm third harmonic of Nd:YAG laser), dihydroxybenzene matrix doped with KBr and fructose, of a mixture of PEG 1000 and PEG 1500, showing quasi-molecular $(M + K)^+$ ions ranging from 850 ≤ m/z ≤ 2,100; bottom, broad-band mass-selective axialization of ions of 1050 ≤ m/z < 1450. Note the sharp selectivity without loss in signal-to-noise ratio.

theoretical basis of the second method[50] is linear response theory which allows application of repeated low-amplitude SWIFT excitations to produce magnetron/cyclotron conversion while maintaining a small "flip angle". This second method has already shown excellent selectivity in axialization of ions over a broad m/z range, as nicely illustrated in Figure 20 by highly mass-selective isolation of ions of 1050 ≤ m/z ≤ 1450 from a poly(ethylene glycol) sample (mixture of PEG 1000 and PEG 5000) originally containing components ranging from ~850 ≤ m/z ≤ 2100. (The ion relative abundances in the two spectra do not match exactly, presumably due to shot-to-shot variation in the laser desorption/ionization process, digital resolution, imperfection in the amplitude uniformity of the broadband axialization excitation, and mass discrimination in transfer from source to analyzer traps.)

In an ICR ion trap with perfectly quadrupolar electrostatic trapping potential and spatially uniform dipolar excitation and detection fields, mass selectivity from *axialization* of ions of desired m/z range(s) should be comparable to that obtained by selective dipolar SWIFT radial *ejection* of ions of the complementary undesired m/z range(s).[77,83-88] Nevertheless, we believe that axialization is preferable for several reasons. First, axialization requires relatively low amplitude excitation voltage to keep ions near the center of the trap, whereas radial ejection requires higher excitation voltage because ions must be driven to the walls of the trap to achieve radial ejection. Second, for the common case that ions of a single or

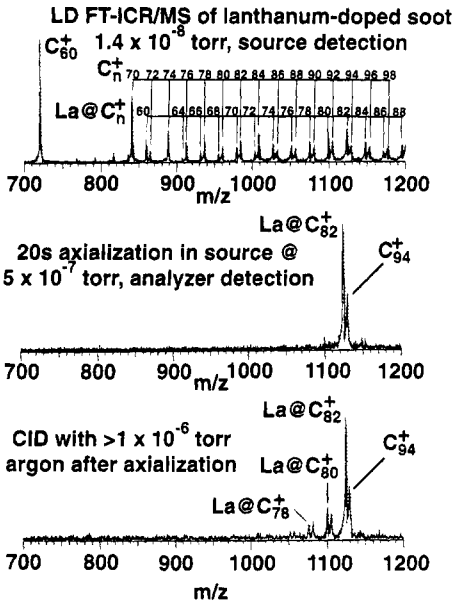


**Figure 21.** CID improved by axialization of parent ions. The top is a FT-ICR mass spectrum of laser-desorbed endohedral fullerene cations, $La@C_n^+$; middle, selective axialization of $La@C_{82}^+$ ions; bottom, FT-ICR mass spectrum following collisional activation by single-frequency dipolar excitation in the analyzer trap—note the loss of $C_2$ units in the product ions, confirming that the La atom is indeed inside the fullerene cage.

very narrow range of m/z values are selected, quadrupolar excitation is narrow band whereas radial ejection is broad band, so that axialization requires even lower amplitude. Third, the axialization mass selectivity demonstrated here was achieved with a relatively large conductance limit aperture (2 mm diameter); higher selectivity could be achieved with a smaller conductance limit aperture.

## D. Improved Collision-Induced Dissociation (CID) Performance

High-mass selectivity for ion isolation is most obviously useful for tandem mass spectrometry (MS/MS) applications. We have improved MS/MS performance by axialization of parent and/or product ions. For example, for parent ion isolation in CID of metal-containing fullerene cations, a broad-band positive-ion Nd:YAG laser desorption/ionization FT-ICR mass spectrum of lanthum-doped fullerene soot shows a variety of fullerene and $La@C_n^+$ ions, 60 ≤ n ≤ 88 (Figure 21, top). From this mixture, $La@C_{82}^+$ ions were selectively axialized in the source side trap while ions of all other m/z were allowed to undergo magnetron expansion. Because the other ions then all have large magnetron radii, only $La@C_{82}^+$ ions survive after subsequent ion transfer to the analyzer trap (Figure 21, middle). Conventional resonant CID experiments may be carried out on the isolated ions by pulsing Ar collision gas in the analyzer trap.[89] Loss of $C_2$ and $C_4$ units to form the products $La@C_{80}^+$ and $La@C_{78}^+$ (Figure 21, bottom) is consistent with an endohedral structure for $La@C_{82}$. In these experiments, no low-mass products are observed, presumably because low-mass product ions are not efficiently trapped because they are formed off-axis and are lost by magnetron expansion at high pressure during

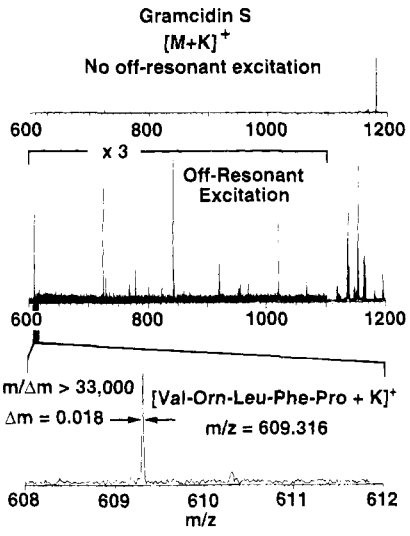


**Figure 22.** CID improved by axialization of product ions. *Top:* Laser-desorbed potassiated gramcidin S ions in the source trap may be axialized and transferred to the analyzer trap for detection. Middle: Sustained off-resonant excitation of the parent $(M + K)^+$ ions with simultaneous broad-band axialization of CID product ions in the source trap makes possible transfer of the product ions to the analyzer trap for high-resolution detection. Bottom: Scale expansion near m/z 610 to show the unprecedented uniformly high resolution (20000–30000) for CID product ions throughout the mass range. (Reprinted from ref 94. Copyright 1994 American Chemical Society.)

pulsed collision gas introduction, and/or because a low-mass product ion acquires high kinetic energy from the collision that formed it, and may be ejected during the final cyclotron excitation event.

In order to dissociate a large biopolymer ion, it is necessary to deposit a large amount of energy into the ion. Off-resonant excitation[90,91] and phase-shifted excitation[92,93] in the presence of collision gas allow ion cyclotron motion to be excited and deexcited periodically, so that the maximum cyclotron radius can be relatively (and controllably) small. During the necessarily long excitation period for either method, product ions may be lost from the trap due to magnetron expansion during excitation at the high collision gas pressure necessary for CID. We have developed a novel CID/axialization method in which the source trap excitation and detection electrodes are connected so as to allow for simultaneous azimuthal quadrupolar and normal dipolar excitation. Isolated parent ions are thereby subjected to off-resonance dipolar excitation while a simultaneous train of SWIFT excitation pulses in quadrupolar mode achieves broad band axialization of product ions spanning a wide m/z range. In this manner, we were able to recover many sequence-specific product ions from CID of potassiated gramicidin S. *Mass-resolving power greater than 20000 has been achieved for product ions over an* m/z *range of 600* (see Figure 22).[94]

Other potential applications of axialization for tandem mass spectrometry include photodissociation and surface-induced dissociation (SID). Because parent ions may be axialized to a small and narrow radial distribution, a laser can be tightly focused on the ions for predicted improved photodissociation efficiency. Of course, trapping of the product ions from either photodissociation or SID could be improved by the axialization method.

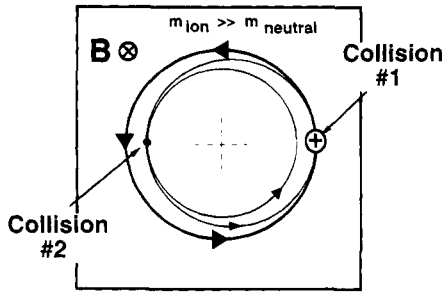


**Figure 23.** Microscopic model for frictional damping of cyclotron motion of heavy ions colliding with light neutrals, if the initial magnetron radius is zero. Following dipolar resonant excitation, ions travel in a large-radius cyclotron orbit (thick circle). The first collision slows the ion but does not significantly change its direction, thereby shrinking the cyclotron radius and shifting its center to the right. A second collision on the opposite side of the cyclotron orbit shrinks the cyclotron radius again and shifts the center to the left. The effect of many such collisions at various phase positions around the cyclotron orbit is to slow the ion by many small steps, so that the ion spirals back to rest at the center of its original cyclotron orbit circle.

## E. Ion Remeasurement

High-mass ions (e.g., laser-desorbed or electrosprayed proteins) are often available only in relatively low numbers. However, following conventional dipolar resonant cyclotron excitation, collisions of high-mass ions with low-mass neutrals have the effect of frictional damping of the cyclotron motion, so that such ions may be reexcited and detected again and again, provided that the initial magnetron radius is zero.[31] The mechanism for the damping is shown in Figure 23. After a heavy ion is excited to a large-radius (~0.5–1.0 cm) cyclotron orbit, a collision with a light neutral slows the ion but does not significantly deflect its direction. The ion cyclotron radius, which is proportional to ion speed, therefore shrinks slightly, and the center of the cyclotron orbit shifts away from the center of the trap to yield a nonzero magnetron radius. However, if the next collision occurs on the other side of the cyclotron orbit (i.e., at 180° different cyclotron phase), then the next shrinkage of the ICR orbital radius shifts the cyclotron orbit center back toward the center of the trap. In the limit that each collision shrinks the cyclotron radius by an amount small compared to that cyclotron radius, the process may be modeled as frictional damping,[25] and the ion trajectory is a spiral of decreasing radius, eventually driving the ion back to the center of the trap, after which the ion may be reexcited and redetected. The preceding argument of course requires that the ion have zero initial magnetron radius; otherwise, the same frictional damping that reduces the cyclotron radius to zero will also exponentially increase the magnetron radius.

From the preceding discussion, it is clear that prior axialization of an ensemble of ions of various initial magnetron radii should greatly improve the efficiency of remeasurement. Speir *et al.*[47] have shown that prior axialization improves the efficiency of remeasurement to >99.5%. For example, Figure 24 shows improvement by a factor of 10 in signal-to-noise ratio

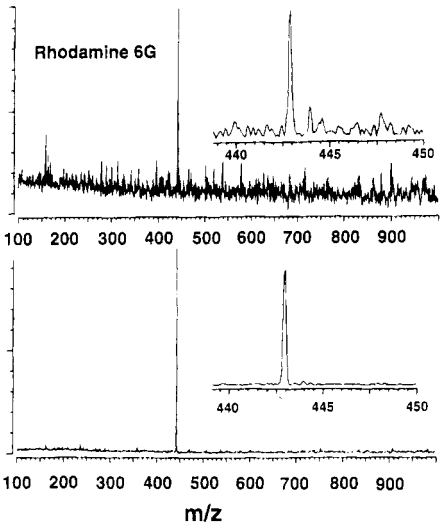


**Figure 24.** Axialization for improved efficiency of ion remeasurement. The top is a FT-ICR mass spectrum of single-shot laser-desorbed rhodamine 6G; bottom, mass spectrum of ions from another single shot following 200 remeasurements, with axialization between each successive remeasurement. The insets show that mass-resolving power is not degraded by the multiple remeasurement process. Note the order-of-magnitude improvement in signal-to-noise ratio. (Reprinted from ref 47. Copyright 1993 American Chemical Society.)

without loss in mass-resolving power for a laser desorption FT-ICR mass spectrum of rhodamine 6G, as a result of 200 remeasurements of the same ions. Alternatively, the same authors also note that several different experiments (e.g., different bandwidths) may be conducted by remeasurement of the same initial ion ensemble.

### F. Ion Capture Efficiency from External Ion Injection

Another obvious application for axialization is for improved efficiency in injection of externally formed ions into an ICR ion trap. The problem is that during injection of ions from a low-current continuous ion beam, the ions which arrive first in the trap begin to diffuse radially outward due to collision-induced magnetron orbit expansion. Thus, by the time later-arriving ions show up, the ions which arrived earlier have leaked out, so that it is impossible to fill the trap with ions even after an indefinitely long injection period. Therefore, it is preferable to fill the trap with ions from a series of pulsed injections (each accompanied by pulsed buffer gas during axialization), as recently demonstrated by Hasse *et al.*[95] for $Au_n^+$ ions, for a continuous beam of electrosprayed ions of a single m/z ratio,[96] and for continuously injected ions of a wide range of m/z ratio.[97,98]

## VI. Conclusions and Future Directions

Ion axialization by quadrupolar excitation/collisional cooling is still a very new technique. Nevertheless, it already has an assured place in the arsenal of FT-ICR techniques for improved signal-to-noise ratio, improved mass-resolving power, extended ion-trapping period for efficient cooling of internally excited ions and study of slow unimolecular processes, higher mass selectivity for MS/MS, higher CID efficiency, improved ion capture efficiency, and higher ion remeasurement efficiency.

Future improvements should include the use of a smaller conductance limit aperture for improved differential pumping and higher mass-resolving power, and use of "shaped-pulse" techniques from FT-NMR spectroscopy for improved broad-band axialization performance. Future applications should include improved efficiency for photodissociation (since ions can be packed closer together to intercept all of the laser beam), as well as direct detection of optical absorption of trapped mass-selected ions. Optically detected magnetic resonance and even direct magnetic resonance detection of mass-selected trapped ions now appear feasible, as we hope to demonstrate experimentally in the near future.

*Acknowledgments.* This work was supported by N.S.F. (CHE-9322824), N.I.H. (GM-31683), The Ohio State University, and The National High Magnetic Field Laboratory at Florida State University. We thank C. Capp and J. V. Coe for supplying fullerene samples.

## References

(1) Marshall, A. G. *Adv. Mass Spectrom.* **1989**, *11A*, 651–668.
(2) Wanczek, K.-P. *Int. J. Mass Spectrom. Ion Processes* **1989**, *95*, 1–38.
(3) Wilkins, C. L.; Chowdhury, A. K.; Nuwaysir, L. M.; Coates, M. L. *Mass Spectrom. Rev.* **1989**, *8*, 67–92.
(4) Freiser, B. S. *Chemtracts–Anal. Phys. Chem.* **1989**, *1*, 65–109.
(5) Ghaderi, S. *Ceram. Trans.* **1989**, *5*, 73–86.
(6) Sharpe, P.; Richardson, D. E. *Coord. Chem. Rev.* **1989**, *93*, 59–85.
(7) Gord, J. R.; Freiser, B. S. *Anal. Chim. Acta* **1989**, *225*, 11–24.
(8) Nibbering, N. M. M. *Acc. Chem. Res.* **1990**, *23*, 279–285.
(9) *Lasers in Mass Spectrometry*; Lubman, D. M., Ed.; Oxford, U. Press: New York, 1990; 545 pp.
(10) Freiser, B. S. In *Bonding Energetics in Organometallic Compounds*; Marks, T. J., Ed.; American Chemical Society: Washington, DC, 1990; Vol. 428; pp 55–69.
(11) Laude, D. A., Jr.; Hogan, J. D. *Techn. Mess.* **1990**, *57*, 155–159.
(12) Cody, R. B., Jr.; Bjarnason, A.; Weil, D. A. In *Lasers in Mass Spectrometry*; Lubman, D. M., Ed.; Oxford Univ. Press: New York, 1990; pp 316–339.
(13) Marshall, A. G.; Grosshans, P. B. *Anal. Chem.* **1991**, *63*, 215A–229A.
(14) Asamoto, B.; Dunbar, R. C. *Analytical Applications of Fourier Transform Ion Cyclotron Resonance Mass Spectrometry*; VCH: New York, 1991; 306 pp.
(15) Nuwaysir, L. M.; Wilkins, C. L. In *Proc. SPIE Applied Spectroscopy in Material Science*; International Society for Optical Engineering: Bellingham, WA, 1991; pp 112–123.
(16) Campana, J. E. In *Proc. SPIE Applied Spectroscopy in Material Science*; International Society for Optical Engineering: Bellingham, WA, 1991; pp 138–149.
(17) Schweikhard, L.; Alber, G. M.; Marshall, A. G. *Phys. Scr.* **1992**, *46*, 598–602.
(18) Marshall, A. G.; Schweikhard, L. *Int. J. Mass Spectrom. Ion Processes* **1992**, *118/119*, 37–70.
(19) Dunbar, R. C. *Mass Spectrom. Rev.* **1992**, *11*, 309–339.
(20) Köster, C.; Kahr, M. S.; Castoro, J. A.; Wilkins, C. L. *Mass Spectrom. Rev.* **1992**, *11*, 495–512.
(21) Speir, J. P.; Gorman, G. S.; Amster, I. J. In *Mass Spectrometry in the Biological Sciences: A Tutorial*; Gross, M. L., Ed.; Kluwer Academic Publishers: Dordrecht, 1992; pp 199–212.
(22) Jacoby, C. B.; Holliman, C. L.; Gross, M. L. In *Mass Spectrometry in the Biological Sciences: A Tutorial*; Gross, M. L., Ed.; Kluwer Academic Publishers: Dordrecht, 1992; pp 95–116.
(23) Stirk, K. M.; Kiminkinen, M.; Kenttämaa, H. I. *Chem. Rev.* **1992**, *92*, 1649–1665.
(24) Nibbering, N. M. M. *Analyst* **1992**, *117*, 289–293.
(25) Schweikhard, L.; Marshall, A. G. *J. Am. Soc. Mass Spectrom.* **1993**, *4*, 433–452.
(26) Buchanan, M. V.; Hettich, R. L. *Anal. Chem.* **1993**, *65*, 245A–259A.
(27) Brenna, J. T.; Creasy, W. R.; Zimmerman, J. *Am. Chem. Soc. Symp. Ser.* **1993**, *236*, 129–154.
(28) Comisarow, M. B. *Int. J. Mass Spectrom. Ion Phys.* **1981**, *37*, 251–257.
(29) Brown, L. S.; Gabrielse, G. *Rev. Mod. Phys.* **1986**, *58*, 233–311.

(30) *Tandem Mass Spectrometry*; McLafferty, F. W., Ed.; Wiley: New York, 1983.
(31) Williams, E. R.; Henry, K. D.; McLafferty, F. W. *J. Am. Chem. Soc.* **1990**, *112*, 6157–6162.
(32) Solouki, T.; Russell, D. H. *Appl. Spectrosc.* **1993**, *47*, 211–217.
(33) Hettich, R. L.; Buchanan, M. V. *Int. J. Mass Spectrom. Ion Processes* **1991**, *111*, 365–380.
(34) Castoro, J. A.; Wilkins, C. L. *Anal. Chem.* **1993**, *65*, 2621–2627.
(35) Beavis, R. C.; Chait, B. T. *Chem. Phys. Lett.* **1991**, *181*, 479–484.
(36) Senko, M. W.; Beu, S. C.; McLafferty, F. W. *J. Am. Soc. Mass Spectrom.* **1993**, *4*, 828–830.
(37) Beu, S. C.; Senko, M. W.; Quinn, J. P.; Wampler, F. M., III; McLafferty, F. W. *J. Am. Soc. Mass Spectrom.* **1993**, *4*, 557–565.
(38) Suckau, D.; Shi, Y.; Beu, S. C.; Senko, M. W.; Quinn, J. P.; Wampler, F. M., III; McLafferty, F. W. *Proc. Natl. Acad. Sci. U.S.A.* **1993**, *90*, 790–793.
(39) Stafford, G. C., Jr.; Kelly, P. E.; Syka, J. E. P.; Reynolds, W. E.; Todd, J. F. J. *Int. J. Mass Spectrom. Ion Phys.* **1984**, *60*, 85–98.
(40) Wineland, D.; Dehmelt, H. *Int. J. Mass Spectrom. Ion Phys.* **1976**, *19*, 251–251.
(41) Wineland, D. J.; Dehmelt, H. G. *Int. J. Mass Spectrom. Ion Phys.* **1975**, *16*, 338.
(42) Van Dyck, R. S., Jr.; Schwinberg, P. B.; Dehmelt, H. G. In *New Frontiers in High Energy Physics*; Kursunoglu, B., Pearlmutter, A., Scott, L. F., Eds.; Plenum Press: New York, 1978; pp 159–181.
(43) Bollen, G.; Moore, R. B.; Savard, G.; Stolzenberg, H. *Appl. Phys.* **1990**, *68*, 4355–4374.
(44) Savard, G.; Becker, S.; Bollen, G.; Kluge, H.-J.; Moore, R. B.; Schweikhard, L.; Stolzenberg, H.; Wiess, U. *Phys. Lett. A* **1991**, *158*, 247–252.
(45) Schweikhard, L.; Guan, S.; Marshall, A. G. *Int. J. Mass Spectrom. Ion Processes* **1992**, *120*, 71–83.
(46) Guan, S.; Wahl, M. C.; Wood, T. D.; Marshall, A. G. *Anal. Chem.* **1993**, *65*, 1753–1757.
(47) Speir, J. P.; Gorman, G. S.; Pitsenberger, C. C.; Turner, C. A.; Wang, P. P.; Amster, I. J. *Anal. Chem.* **1993**, *65*, 1746–1752.
(48) Guan, S.; Marshall, A. G. *Rapid Commun. Mass Spectrom.* **1993**, *7*, 857–860.
(49) Guan, S.; Wahl, M. C.; Marshall, A. G. *Anal. Chem.* **1993**, *65*, 3647–3653.
(50) Guan, S.; Marshall, A. G. *J. Chem. Phys.* **1993**, *98*, 4486–4493.
(51) Guan, S.; Wahl, M. C.; Marshall, A. G. *J. Chem. Phys.* **1994**, *100*, 6137–6140.
(52) Guan, S.; Xiang, X.; Marshall, A. G. *Int. J. Mass Spectrom. Ion Processes* **1993**, *124*, 53–67.
(53) Wobschall, D.; Graham, J. R., Jr.; Malone, D. P. *Phys. Rev.* **1963**, *131*, 1565–1571.
(54) Beauchamp, J. L. *J. Chem. Phys.* **1967**, *46*, 1231–1243.
(55) Wang, M.; Marshall, A. G. *Anal. Chem.* **1990**, *62*, 515–520.
(56) Hanson, C. D.; Castro, M. E.; Kerley, E. L.; Russell, D. H. *Anal. Chem.* **1990**, *62*, 520–526.
(57) Caravatti, P.; Allemann, M. *Org. Mass Spectrom.* **1991**, *26*, 514–518.
(58) Grosshans, P. B.; Chen, R.; Marshall, A. G. *Int. J. Mass Spectrom. Ion Processes* **1994**, in press.
(59) Pan, Y. P.; Ridge, D. P.; Rockwood, A. L. *Int. J. Mass Spectrom. Ion Processes* **1988**, *84*, 293.
(60) Nikolaev, E. N.; Gorshkov, M. V.; Mordehai, A. V.; Talrose, V. L. *Rapid Commun. Mass Spectrom.* **1990**, *4*, 144–146.
(61) Limbach, P. A.; Grosshans, P. B.; Marshall, A. G. *Int. J. Mass Spectrom. Ion Processes* **1993**, *123*, 41–47.
(62) Yin, W. W.; Wang, M.; Marshall, A. G.; Ledford, E. B., Jr. *J. Am. Soc. Mass Spectrom.* **1992**, *3*, 188–197.
(63) Wanczek, K.-P.; Wang, Y. *J. Chem. Phys.* **1993**, *98*, 2647–2652.
(64) Wang, M.; Marshall, A. G. *Anal. Chem.* **1989**, *61*, 1288–1293.
(65) Jackson, J. D. *Classical ELectrodynamics*; Wiley: New York, 1975; 848 pp.
(66) March, R. E.; Hughes, R. J. *Quadrupole Storage Mass Spectrometry*; Wiley: New York, 1989; 471 pp.
(67) Francl, T. J.; Fukuda, E. K.; McIver, R. T., Jr. *Int. J. Mass Spectrom. Ion Processes* **1983**, *50*, 151–167.
(68) Xiang, X.; Guan, S.; Marshall, A. G. *J. Am. Soc. Mass Spectrom.* **1994**, *5*, 238–249.
(69) Xiang, X.; Marshall, A. G. *J. Am. Soc. Mass Spectrom.* **1994**, *5*, 807–813.
(70) Guan, S. *J. Chem. Phys.* **1992**, *96*, 7959–7964.
(71) Freeman, R. *Chem. Rev.* **1991**, *91*, 1397–1412.
(72) Rosen, N.; Zener, C. *Phys. Rev.* **1932**, *40*, 502.
(73) Warren, W. S.; Silyer, M. S. *Adv. Magon. Res.* **1988**, *12*, 247–384.
(74) Baum, J.; Tycko, R.; Pines, A. *Phys. Rev. A* **1985**, *32*, 3435–3447.
(75) Chen, R.; Guan, S.; Marshall, A. G. *J. Chem. Phys.* **1994**, *100*, 2258–2266.
(76) Chen, L.; Wang, T. C. L.; Ricca, T. L.; Marshall, A. G. *Anal. Chem.* **1987**, *59*, 449–454.
(77) Guan, S.; McIver, R. T., Jr. *J. Chem. Phys.* **1990**, *92*, 5841–5846.
(78) Marshall, A. G.; Comisarow, M. B.; Parisod, G. *J. Chem. Phys.* **1979**, *71*, 4434–4444.
(79) Guan, S.; Marshall, A. G. *J. Am. Soc. Mass Spectrom.* **1994**, *5*, 64–71.
(80) Rempel, D. L.; Gross, M. L. *J. Am. Soc. Mass Spectrom.* **1992**, *3*, 590–594.
(81) Wood, T. D.; Schweikhard, L.; Marshall, A. G. *Anal. Chem.* **1992**, *64*, 1461–1469.
(82) Wahl, M. C.; Kim, H. S.; Wood, T. D.; Guan, S.; Marshall, A. G. *Anal. Chem.* **1993**, *65*, 3669–3676.
(83) Marshall, A. G.; Wang, T.-C. L.; Ricca, T. L. *J. Am. Chem. Soc.* **1985**, *107*, 7893–7897.
(84) Marshall, A. G.; Wang, T.-C. L.; Chen, L.; Ricca, T. L. *Am. Chem. Soc. Symp. Ser.* **1987**, *359*, 21–33 (M. V. Buchanan, Ed.).
(85) Guan, S. *J. Am. Soc. Mass Spectrom.* **1991**, *2*, 483–486.
(86) Guan, S. *J. Chem. Phys.* **1990**, *93*, 8442–8445.
(87) Guan, S. *J. Chem. Phys.* **1989**, *91*, 775–777.
(88) Grosshans, P. B.; Marshall, A. G. *Anal. Chem.* **1991**, *63*, 2057–2061.
(89) Wood, T. D.; Ross, C. W., III; Marshall, A. G. *J. Am. Soc. Mass Spectrom.* **1994**, *5*, 900–907.
(90) Beauchamp, J. L. *Annu. Rev. Phys. Chem.* **1971**, *22*, 527–561.
(91) Gauthier, J. W.; Trautman, T. R.; Jacobson, D. B. *Anal. Chim. Acta* **1991**, *246*, 211–225.
(92) Boering, K. A.; Rolfe, J.; Brauman, J. I. *Rapid Commun. Mass Spectrom.* **1992**, *6*, 303–305.
(93) Boering, K. A.; Rolfe, J.; Brauman, J. I. *Int. J. Mass Spectrom. Ion Processes* **1992**, *117*, 357–386.
(94) Guan, S.; Marshall, A. G.; Wahl, M. *Anal. Chem.* **1994**, *66*, 1363–1367.
(95) Hasse, H. U.; Becker, S.; Dietrich, G.; Klisch, N.; Kluge, H. J.; Lindinger, M.; Lutzendirchen, K.; Schweikhard, L.; Ziegler, J. *Int. J. Mass Spectrom. Ion Processes* **1994**, *132*, 181–191.
(96) Bruce, J. E.; Anderson, G. A.; Hofstadler, S. A.; Van Orden, S. L.; Sherman, M. S.; Rockwood, A. L.; Smith, R. D. *Rapid Commun. Mass Spectrom.* **1993**, *7*, 914–919.
(97) Marto, J. A.; Guan, S.; Marshall, A. G. *Rapid Commun. Mass Spectrom.* **1994**, *8*, 615–620.
(98) Guan, S.; Paša-Tolić, L.; Marshall, A. G.; Xiang, X. *Int. J. Mass Spectrom. Ion Processes*, in press.